Ultrastructural Characterization of Individual Myofibrils Using Second Harmonic Generation

By Caylee Alexandra MacDonald

A Thesis Submitted to

Saint Mary's University, Halifax, Nova Scotia

In Partial Fulfillment of the Requirements for the Degree of Bachelor of Science with Honours in Chemistry

April 2024, Halifax, Nova Scotia

Supervisor: Dr. Danielle Tokarz

Department Chair: Dr. Clarissa Sit

Date: April 22, 2024

Certification

Ultrastructural Characterization of Individual Myofibrils Using Second Harmonic Generation

By: Caylee Alexandra MacDonald

I hereby certify that this thesis was completed by Caylee Alexandra MacDonald in partial fulfillment of the requirements of the Degree of Bachelor of Science with Honours in Chemistry at Saint Mary's University and I certify that this is truly original work carried out by Caylee Alexandra MacDonald.

Thesis Supervisor

_____

Chairperson of the Chemistry Department

_____

Date: April 22, 2024

Abstract

Ultrastructural Characterization of Individual Myofibrils Using Second Harmonic Generation

Second harmonic generation (SHG) is a non-linear optical effect in which two identical incident photons interact with a material to generate one photon at twice the frequency of one incident photon. Polarization-resolved second harmonic generation microscopy (PSHG) has been used in biomedical research to study collagen, muscle, and a variety of other biological tissues. In this work individual myofibrils were imaged with PSHG microscopy, and the optical parameter ρ, which is related to molecular disorder, is reported. The relationship between contractile state of individual myofibrils and ρ was also investigated.

The results of this study show that individual myofibrils dissected from *Drosophila melanogaster* can be successfully imaged using PSHG. Individual myofibrils dissected and fixed at physiological ATP concentration and imaged in water were found to have a mean ρ value of 0.544 ± 0.03. A gradient in ρ value perpendicular to the direction of the sarcomere was observed in fibrils in this population. In the A-band, I-band, and M-line of the sarcomere the average ρ values are reported in both the relaxed and rigor state. The mean ρ value of the A-band was found to be significantly higher than the M-line and I-band in the relaxed state. In the contracted state the level of disorder in the three regions was not significantly different. The level of disorder increased in all three regions as ATP concentration decreased.

Acknowledgements

I would first like to thank my supervisors Dr. Danielle Tokarz and Dr. Richard Cisek for providing me with the opportunity to carry out this research in their lab. Their expert knowledge, dedication to their students, and passion for research made this project a wonderful experience. I would also like to thank my group members MacAulay Harvey, Elisha Bennett, Breanna Lane, Katie Zinck, and Sasha MacArthur for their encouragement and support throughout this project. MacAulay's research on collagen fibrils laid the groundwork for this myofibril research, and his findings have been extremely helpful. I am grateful for the opportunity to work in the collaborative research environment fostered within the Tokarz Research Group. I would also like to thank SMUWorks for providing the funding for research carried out for this project last summer.

I would like to thank my collaborators at Dalhousie University, Dr. Nicanor Gonzalez-Morales, Dr. Laurent Kreplek, and Jennifer Johnson. I am grateful for the opportunity to use their equipment and for their expert knowledge and advice.

I would like to thank my Honours Seminar professor Dr. Robert Singer and my Honours Thesis professor Dr. Jason Masuda for their guidance throughout this project. I would like to thank my Honours classmates Deana Symes and Lauryn Mason for their support and friendship. Additionally, I am grateful to the SMU Chemistry Department faculty for their helpful feedback on my progress report and their willingness to discuss research with me.

Finally, I would like to thank my family and friends for their love and support throughout my degree. I would especially like to thank my parents Dianna and Joseph MacDonald for inspiring curiosity and the desire to learn, which has been my greatest inspiration throughout my research journey.

Table of Contents

List of Figures

List of Tables

List of Equations

List of Abbreviations

SHG	Second harmonic generation
ρ	Level of disorder
AMI	Acute myocardial infarction
ECG	Electrocardiogram
CT	Computed tomography
LMM	Light meromyosin
HMM	Heavy meromyosin
S1	Myosin head
S2	Myosin neck
A-band	Anisotropic band
I-band	Isotropic band
ATP	Adenosine triphosphate
P_i	Inorganic phosphate
$\chi^{(2)}$	Second Order Nonlinear Optical Susceptibility
PIPO	Polarization-in polarization-out
SL	Sarcomere length
SM	Scanning mirror
PSG	Polarization state generator
PSA	Polarization state analyzer
PMT	Photomultiplier tube
2PEF	Two photon excitation fluorescence

1.0 Introduction

1.1 Motivation

Acute myocardial infarction (AMI) is the necrosis of heart muscle tissue due to obstruction in a coronary artery.[1] Also known as a heart attack; AMI is the leading cause of death for American women.[2] Effective treatment of AMI is time sensitive, and yet studies show that women are significantly less likely to seek timely treatment for AMI symptoms.[2]

The main cause of myocardial infarction is ischemia, which is a reduction of the typical blood flow to the heart muscle. Ischemia is primarily diagnosed by electrocardiogram (ECG).[3] Other methods for ischemia diagnosis include a stress test, an echocardiogram, coronary angiography, and a cardiac computed tomography (CT) scan.[4] In a study of ~42 000 participants, the ECG did not provide a definitive diagnosis of ischemia in 93% of patients.[3] Stress tests are known to have low sensitivity and specificity for ischemia, and little research exists on the effects of female hormones on the results of this test.[5] Additionally, the Women's Ischemia Syndrome Evaluation found that 37% of female ischemia patients presented with normal angiograms, which is an imaging technique showing blood flowing through the heart.[5] When the ECG does not yield a diagnosis, it is the responsibility of the physician to determine if ischemia is present based on symptoms and family history.[3] It was found that physicians were then more likely to diagnosis possible ischemia in men than in women (44.5% vs 39%), as the symptoms of ischemia in women are different than those in men, and are less understood.[3]

This study will investigate second harmonic generation microscopy as a tool to observe the molecular changes that occur in myofibrils after an ischemic event, but before a myocardial infarction. With a better understanding of the effects of ischemia at the myofibril level, there is

potential for standardized and efficient diagnosis before a heart attack occurs, which can bridge the gender gap in heart attack diagnosis.

Muscle cells are composed of small fibrils called myofibrils, which are a string of repeating contractile units called sarcomeres. It has been observed that the contraction state of cardiac myofibrils after an ischemic event correlate with reduced ATP and an increased H^+ concentration, displacing Ca^{2+} from the troponin binding site.[6] At an ATP concentration of 2μmol/g the theoretical lower limit of resuscitation is reached, and at levels lower than 5.5 μmol/g a significant decrease in contraction is observed.[6] Because changes in pH and ATP concentration from ischemia are known to affect the contractile state of myofibrils, it is important to develop an imaging technique that will correlate these variables and sarcomere length.

1.2 Muscle Structure

Skeletal muscle is an essential dynamic tissue accounting for ~40% of human body weight, and 50-75% of all body proteins.[7] Muscle is composed of 75% water, 20% proteins, and 5% inorganic salts, carbohydrates, fats, and minerals.[7] The main function of skeletal muscle is the conversion of chemical energy into mechanical energy to generate the force required for movement.

A muscle is composed of a bundle of muscle fibres called fascicles. Each muscle fibre is approximately 100 μm in diameter and 1cm long.[7] Muscle fibres are singular muscle cells and are surrounded by a cell membrane referred to as the sarcolemma.[7] Each muscle fibril is comprised of thousands of myofibrils, which are long contractile fibres.[7]

Within a myofibril are myofilaments, proteins such as actin and myosin, that are organized into sarcomeres, the contractile units of muscle. The myosin motor protein is composed of a static

region, the light meromyosin (LMM), and a dynamic region, the heavy meromyosin (HMM), as shown in Figure 1.[8] Within the HMM there is a myosin head (S1 region) where ATP hydrolysis and actin binding occur.[8] There is also a rod-shaped region, dubbed S2, which is a coiled-coil macrostructure connecting the LMM and S1.[8]

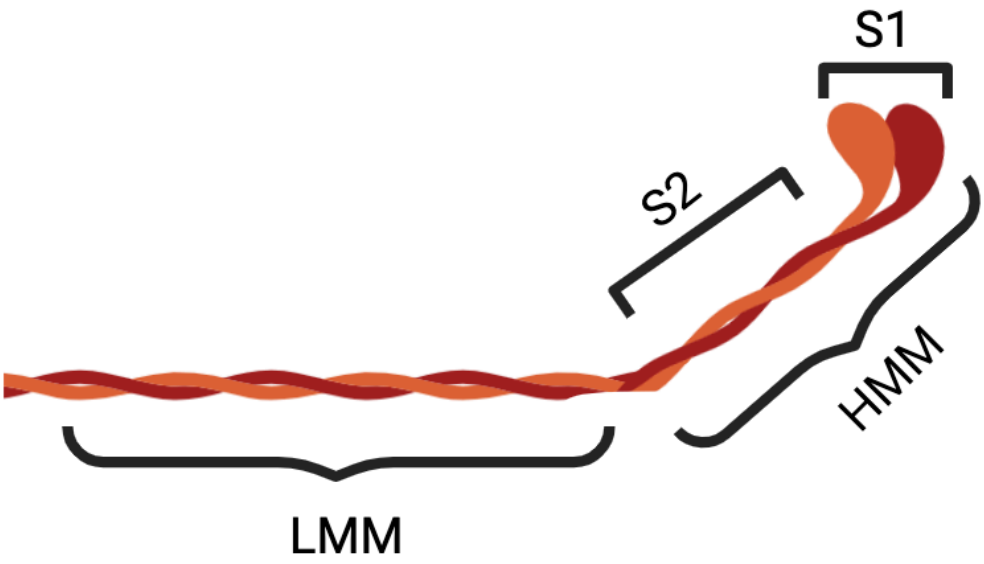

Figure 1: A macromolecular structure of two myosin dimers showing the heavy meromyosin (HMM) and light meromyosin (LMM) regions. The S1 and S2 regions are also shown. The alpha helix coiling at the S2 and LMM regions can be seen. Figure created in BioRender.

Another important protein in muscle is titin, which attaches myosin to the end of each sarcomere, or Z-disk.[7] The Z-disk is composed of proteins such as α-actinin, and is an anchor point for myofilaments in a sarcomere, as well as for proteins connecting to the extracellular matrix and sarcolemma.[7]

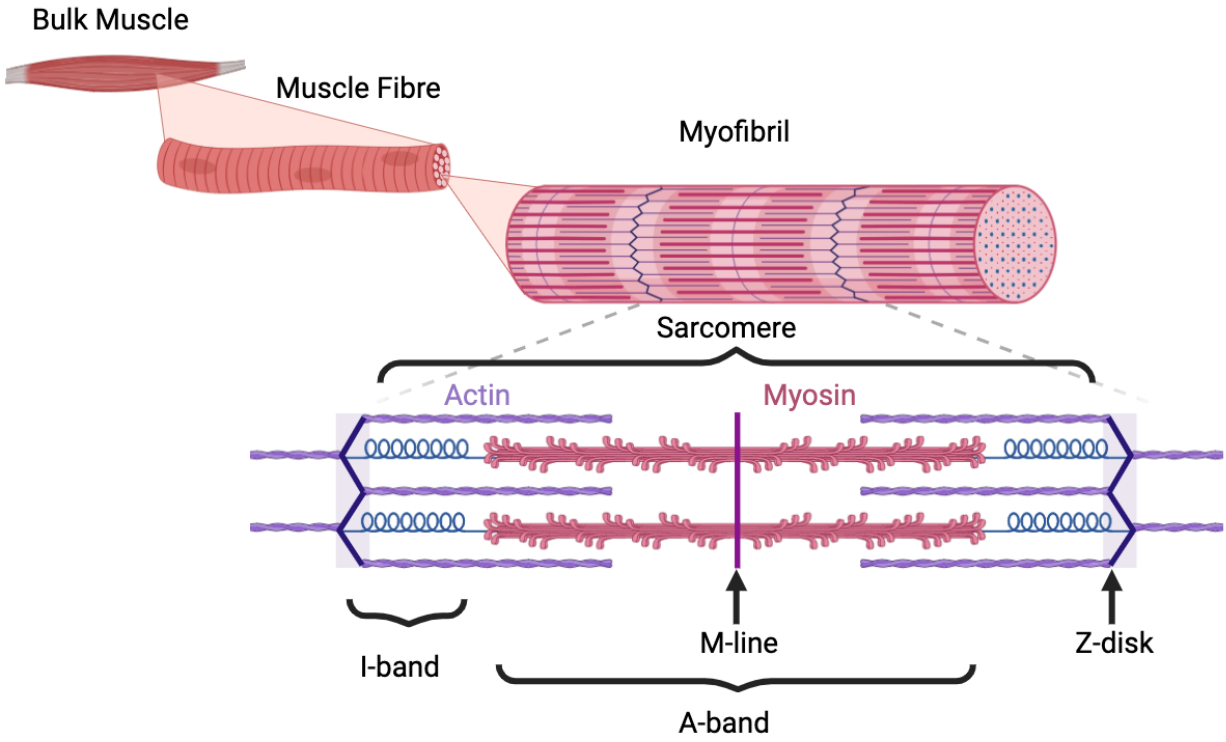

Figure 2: The structural organization of muscle and the regions of a sarcomere. Figure created in BioRender.

Actin and myosin filaments make up 70-80% of the protein content in a muscle fibre.[7] The actin and myosin connect through globular regions of myosin heads that form cross bridges and generate force through hydrolysis of adenosine triphosphate (ATP). Myosin is composed of two heavy chains (220-kD), and two light chains (15-22kD).[9] Each heavy chain of myosin forms a globular head and connects to another filament to make a 'tail' region.[9] The head, or S1 region, is composed of one ATP, actin, two light chains, and a myosin heavy chain. Electron micrographs have shown the myosin head to be 190Å long and 50Å wide.[9] The light chains of myosin are not involved in the ATP hydrolysis activity of the head.[9]

The myosin tail is composed of two myosin alpha helices in a coiled-coil structure.[9] This structure is composed of two right-handed alpha helices that coil together into a left-handed helix.[9]

Each helix is composed of seven amino acid repeats, with the hydrophobic residues pointing inward, and the polar residues exposed on the outside of the helix.[9] Using second harmonic generation microscopy the helical pitch angle of myosin was found to be 62°.[10]

1.2.1 Muscle Contraction

During muscle contraction actin and myosin filaments slide past each other, shortening the sarcomere by pulling the Z-disks together.[7] This concept, known as the sliding filament theory, was first described in 1954.[7] Contraction begins when a nervous impulse is sent to the transverse tubular system, a network of tubules in the sarcolemma that connect to the exterior of the muscle cell and spread the impulse uniformly over a muscle fibre.[7] Receptors on the tubules open and allow calcium to flow into the sarcoplasm.[7] This calcium binds to the troponin protein on actin and tropomyosin is removed from the active site of actin, allowing the myosin head access to this binding site.[7] This process is shown in Figure 3.

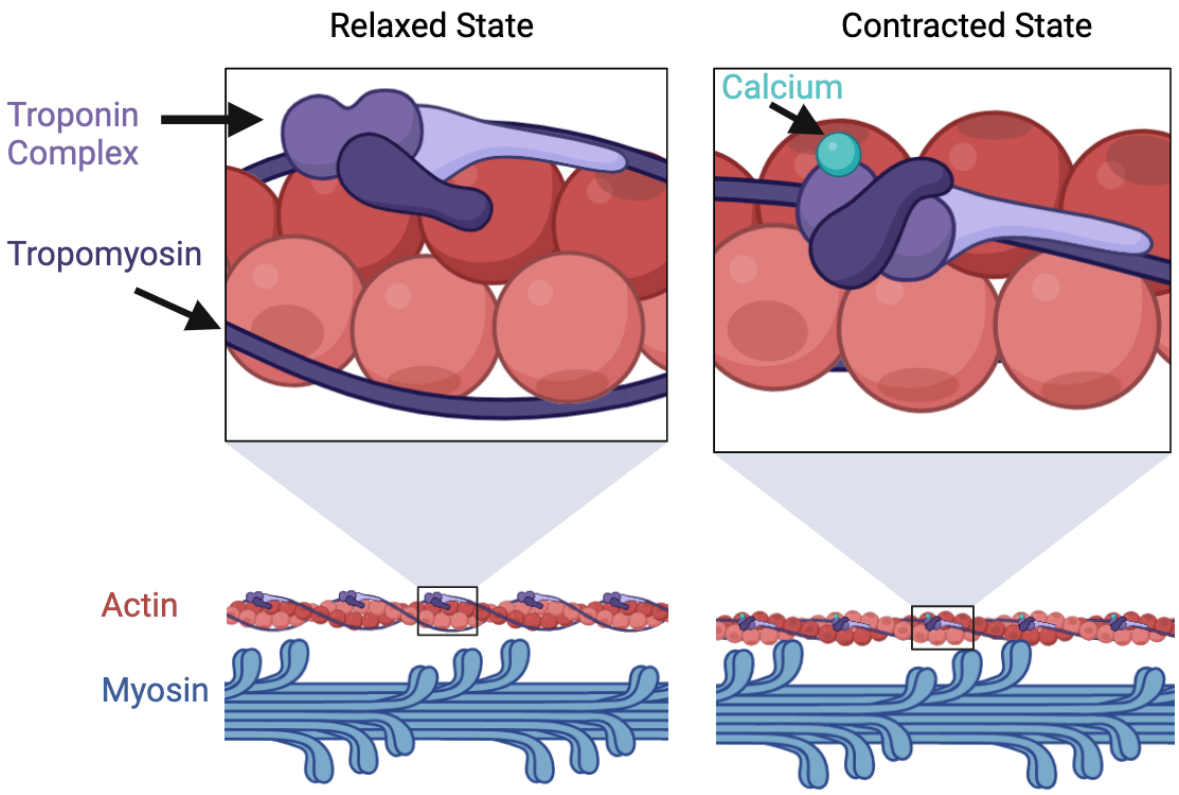

Figure 3: A simplified schematic of the process of muscle contraction showing the binding of troponin to actin. This displaces tropomyosin, leading to an interaction between actin and myosin that generates contraction. Figure created in BioRender.

The energy required for muscle contraction is generated through the ATPase cycle (Figure 4), in which myosin cycles between actin-attached and actin-detached states based on the hydrolysis of ATP.[11] The cycle begins with the ATP molecule attached to myosin undergoing hydrolysis to become P_i-ADP.[7,11] This causes a conformational change in myosin, which allows the head to detach from the currently bound actin, and swing to bind weakly to a new actin filament.[7] The inorganic phosphate (P_i) is then released, and the myosin-ADP structure can bind strongly to actin.[11] This is the rate determining step of this reaction cycle.[11] The S1 domain of the myosin then undergoes a conformational change, and this 'working step' generates contraction.[11] During the

working step myosin pushes the actin filament to move it closer to the opposing Z-disk.[7] This force is transmitted longitudinally and laterally.[7]

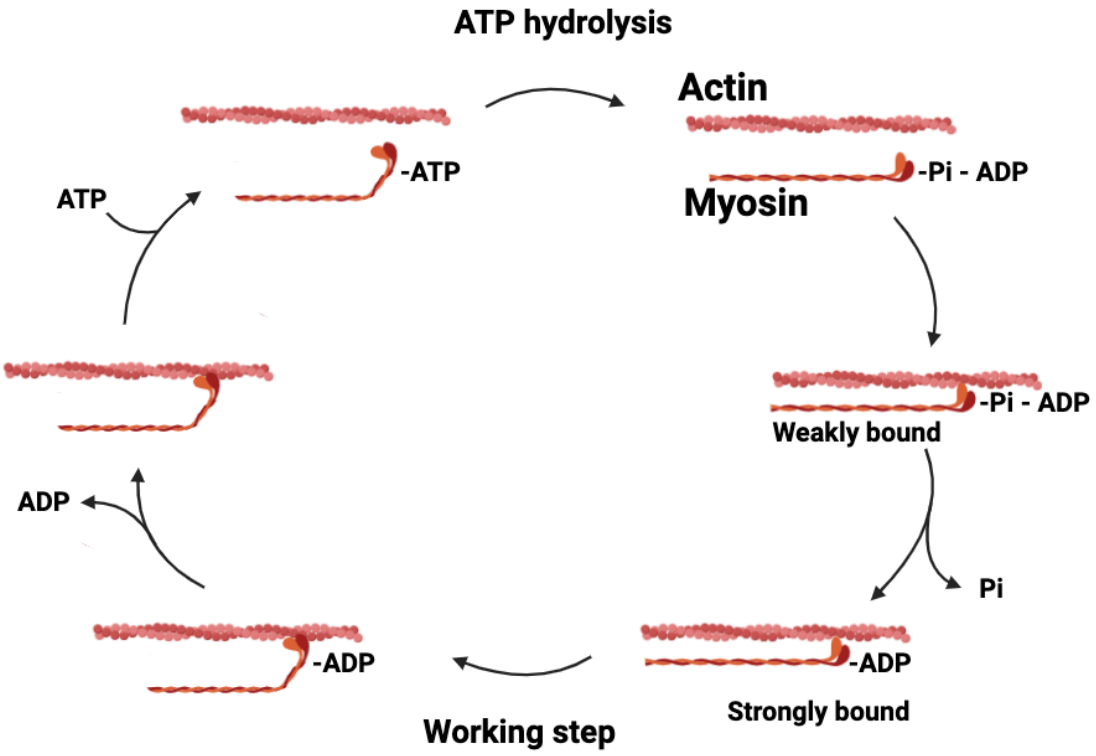

Figure 4: The ATPase cycle showing the interaction of actin and myosin based on ATP hydrolysis. In the working step a conformational change causes contraction of muscle sarcomeres.[11] Figure was created in BioRender.

Rigor mortis is the stiffening of muscle tissue after death.[10] This is caused by a decrease in ATP and Ca^{2+} concentration.[12] When skeletal muscle is in *rigor* all myosin heads are bound to actin, causing an overlap between the thick and thin filaments.[8] When ATP concentration is below 15-20 μmol/g, full-*rigor*, the maximum amount of muscle stiffening is achieved.[12] *Rigor mortis* can be quantified by a rigor index, which increases as pH, muscle glycogen and ATP concentration

decrease.[12] In this study rigor will be induced by decreasing the concentration of ATP to simulate contraction.

1.3 Second Harmonic Generation Theory

Second harmonic generation (SHG) occurs when two photons with the same frequency are excited to a virtual state, and immediately relax to the ground state as one photon with twice the incident frequency, as shown in Figure 5.[13] Harmonic generation can be described by Equation 1, where E represents the electric field of laser light, and P represents the polarization induced by this electric field. $\chi^{(2)}$ is a tensor of rank three containing a maximum of eighteen elements that describe second harmonic generation.[13] The intensity of SHG generated is proportional to $(\chi^{(2)}E^2)^2$.[13]

$$P \propto \chi^{(1)}E^1 + \chi^{(2)}E^2 + \ldots, \qquad (1)$$

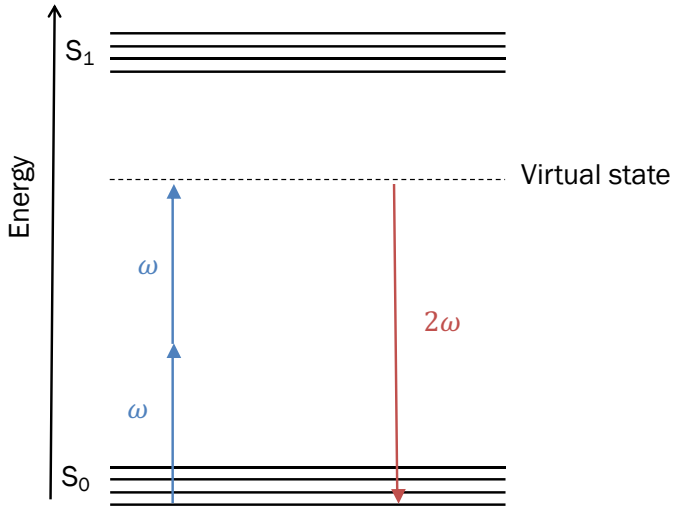

Figure 5: Energy diagram depicting second harmonic generation. Two incident photons of same frequency (ω) are excited to a virtual state. This results in a single photon at twice the incident frequency relaxing back to the ground state. [13]

The molecular structure of this sample must be non-centrosymmetric, which has been demonstrated by the cancellation of signal in symmetrically distributed membranes.[14] It has been shown that when two-photon excitation fluorescence and SHG intensity images of the same vesicle membranes are compared, SHG signal is cancelled in locations of symmetric overlap.[13,14] If cylindrical symmetry is assumed, $\chi^{(2)}$ can be simplified to two terms: $\chi^{(2)}_{zzz}$ and $\chi^{(2)}_{zxx}$. The ratio of $\chi^{(2)}_{zzz}/\chi^{(2)}_{zxx}$ gives a parameter called ρ.[13]

The ρ ratio is related under some assumptions to the helical pitch of a molecule, as shown in 6.[10,13] Assuming that the SHG emitters are oriented at a fixed angle from the cylindrical axis, ρ can be determined by Equation 2.[13] In muscle, the measured ρ value increases with disorder of the helical pitch.[10,13]

$$\frac{\rho}{2+\rho} = \cos 2\ \theta_0 \qquad (2)$$

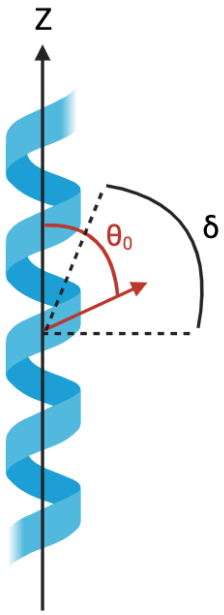

Figure 6: The helical pitch angle in comparison to a central axis. θ_0 represents the helical pitch, and δ represents the disorder in the helical pitch.[10] Figure adapted from Tiaho, 2007, and generated in BioRender.[10]

SHG microscopy has several advantages over fluorescence imaging. Due to the excitation of photons only to a virtual state, no Stokes shift occurs and therefore no heat is released into the sample.[15] Additionally, no staining of the sample is required.[15,16] With SHG microscopy excellent sample penetration can be achieved because this phenomenon occurs in the 'biological window' at 1000nm-1300nm where biological molecules typically do not absorb. Because the photons can travel farther without being absorbed, deeper sample penetration can be achieved. Using polarization resolved SHG microscopy, intrinsic structural determination can be achieved.

1.4 Second Harmonic Generation-Based Quantification of Muscle

The source of second harmonic generation (SHG) from muscle tissue has been elucidated through biochemical analysis and optical imaging. Initially it was theorized that SHG emission is

a result of the crystalline order of the actin-myosin complex.[17] During contraction the actin filament slides along the myosin, causing a decrease in the length of the isotropic band (I-band), which contains only actin.[17] The length of the anisotropic band (A-band) remains unchanged, but the overlap of actin and myosin within this region does change. Using simultaneous SHG and multi-photon excitation fluorescence (generated from fluorescently labelled actin-only regions), it has been shown that the SHG signal is generated from the A-band.[17]

A shrinking and disappearance of I-bands has also been observed in SHG imaging of contracting myocytes.[17] SHG intensity is diminished during contraction, but because the myosin remains in this region it is suggested that the crystalline arrangement of myosin in the A-band determines SHG intensity.[17] It was proposed that there is a decrease in crystalline order during contraction due to relaxation of the myosin heads and conformational changes in tropomyosin and troponin.[17] This suggests that a change in actin overlap with the myosin determines the crystalline order.

However, this theory was later disproven by evidence showing that SHG is generated from myosin only. The results of a 2007 study showed that the Z-line and thin filaments do not emit SHG, and that there is a decrease in SHG signal at the M-line.[18] This was determined through simultaneous imaging of SHG, two photon excitation fluorescence (2PEF), and fluorescent immunostaining of α-actinin or actin. These images were overlaid and the bright and dark SHG regions were found to correlate to specific sarcomere regions.[18] It was found that SHG signal corresponds to the centre of a sarcomere, where the myosin is located.[18] To determine if SHG signal from myosin relies on interaction with actin, the lengths of sarcomeres were correlated with SHG signal. It was found that the SHG emission is not dependant on actin-myosin overlap, and that the SHG signal diameter and peak spacing do not change with sarcomere length.[18] It was also

shown that SHG signal originates in the rod-like myosin tail region and is independent of the orientation of the myosin heads.[18]

A decrease in SHG signal at the M-line has been observed in many studies. Prent et al. hypothesised that this may be due to the lack of myosin heads in the region, or that SHG is not generated in myosin rod regions.[19] It was found that in stretched muscle the dark region between A-bands became smaller or disappeared completely.[19] This changes the region from a double-peak profile to a single peak when stretched.[19] The change from a double intensity peak to a single peak increased from a 15% occurrence in unstretched to 80% in stretched tissue.[19] Their work presents evidence that the decrease in signal is the result of oppositely oriented myosin molecules weakening the degree of non-centrosymmetry.[19]

The change in average SHG intensity has also been observed for a live contracting myocyte, and it was found that average SHG of a sarcomere increases with sarcomere length.[19] This result contradicts the assumption that as a sarcomere is stretched the A-bands are pulled apart.[19] The increase in intensity was explained by the separation of oppositely arranged myosin molecules creating better phase matching conditions.[19] This was explained by the antiparallel arrangement of myosin molecules in the center of the A-bands becoming less ordered.[19]

1.4.1 Polarization-resolved Second Harmonic Generation of Muscle

Polarization-in polarization-out second harmonic generation (PIPO SHG) microscopy involves collecting SHG intensity at the input and output polarization.[20] A two-dimensional plot of input vs output polarization is obtained from this method. This plot can then be fit to an equation by assuming a cylindrical model to determine the ρ value at each pixel.[20] Examples of 2D PIPO plots are shown in Figure 7. Assuming cylindrical symmetry of the fibril, the ρ ratio

represents the orientation distribution of the helical pitch and is related to the degree of molecular disorder.[13]

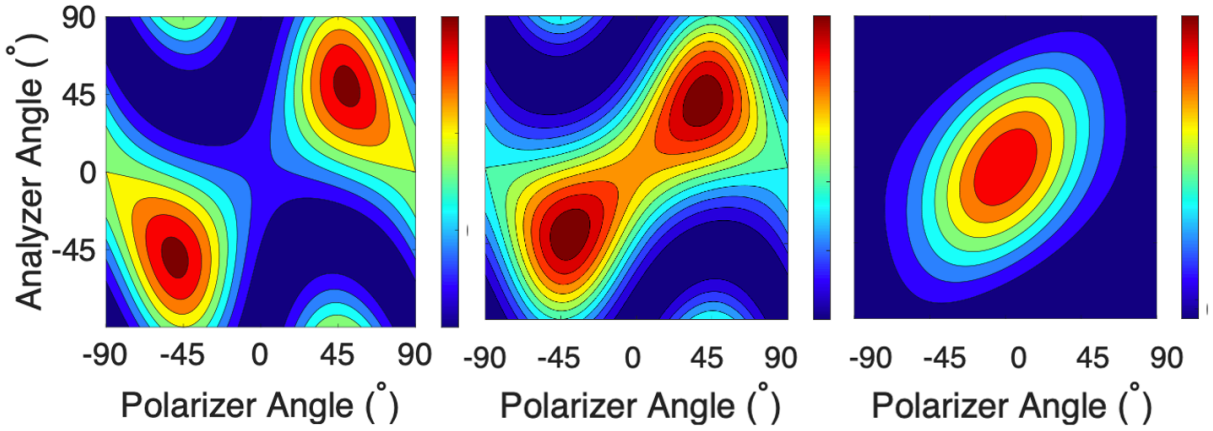

Figure 7: Examples of 2D PIPO bubbles obtained by plotting the polarization-in against the polarization-out. The image on the left shows a typical PIPO bubble from imaging muscle, which has a ρ ratio around 0.5. The middle shows a PIPO bubble from collagen, with a ratio around 2. The plot on the right is an example of a PIPO bubble from starch, which has a ρ ratio around 4. These images were generated through simulation in MATLAB using a custom program.

PIPO SHG microscopy has been used to observe the variation in ρ value in different regions of the sarcomere in muscle tissue in both rats and fruit flies.[20] The M-line is mainly composed of the antiparallel LMM region with no myosin heads.[20] In this region the alpha helices of myosin are mainly aligned along the fibril axis, and so a lower ρ value is expected.[20] The edges of the A-band and the I-band are mainly composed of the HMM, as the myosin heads are oriented along the edges of the filament.[20] In the S1 and S2 regions of the HMM the alpha helices of myosin deviate more from the axis of the fibril, explaining the increase in ρ. [20]

The ρ value was expected to be different on the edges and middle of the A-band because the myosin heads are located along the periphery of myofilaments.[20] This was found to be true, with a mean ρ value at the M-line of 0.489 ± 0.001, and a mean ρ value at the edges of the A-band of 0.498 ± 0.001.[20] This is a difference of ~2%. The I-band had an average ρ value of 0.519 ±

0.001.[20] These results suggest that the HMM and LMM regions of myosin have different ρ values.[20]

Using polarization-in SHG microscopy, Nucciotti et al. observed a relationship between ρ and sarcomere length (SL).[8] In rabbit the average ρ value of *rigor* muscle was found to be 0.68 ± 0.01, and relaxed muscle was found to have a ratio of 0.46 ± 0.03.[8]

The number of heads attached to actin changes with sarcomere length, in accordance with the ATPase cycle shown in Figure 4. With shorter sarcomere length there is a greater number of myosin heads bound to actin, generating contraction. Therefore, the ρ value for muscle in rigor mortis should depend on the degree of contraction (corresponding to more disorder).[8] It was found that average ρ increased as sarcomere length decreased in the rigor state, and that in the relaxed state there is no relation between sarcomere length and ρ.[8]

1.5 Objectives of Thesis

The goal of this project is to investigate whether structural changes in myosin from contraction can be observed using second harmonic generation microscopy. The contraction state of myofibrils will be manipulated through ATP concentration. As ATP concentration has shown to decrease after an ischemic event, understanding corresponding structural changes in individual myofibrils can be applied to cardiac medicine. AMI is the leading cause of death in American women, but studies on imaging contracted muscle can be used to develop new diagnostic and treatment techniques.

The objective of this study will be achieved through imaging of individual myofibrils, as PIPO SHG of individual myofibrils has yet to be reported. The myofibrils will be collected from the

indirect flight muscle of *Drosophila melanogaster*. Like in heart muscle, the contractions of the *Drosophila* indirect flight muscle function to generate power in an oscillatory manner and has therefore been used to study heart disease.[5] It is hypothesized that the level of molecular disorder, the ρ ratio, will change as a sarcomere contracts, and thus a relationship between ρ and sarcomere length can be discerned.

2.0 Experimental

2.1 Sample Preparation

The following protocol for dissection of wildtype Oregon Red *Drosophila melanogaster* was performed by PhD candidate Jennifer Johnson in the lab of Dr. Nicanor Gonzales-Morales at Dalhousie University and assisted by me.

A dissection buffer was prepared by first combining 1mL of 1M sodium phosphate, 500µL of 0.5M magnesium chloride, 1mL of 250mM ethylene glycol-bis(β-aminoethyl ether)-N,N,N′,N′-tetraacetic acid, 2.5mL of 0.1M adenosine triphosphate (ATP), and 50mL of deionized water. 25mL of this solution was then combined with 25mL of glycerol, 1.25 mL of 0.1M of ATP, and 0.05% of Tween detergent to create the dissection buffer.

The *Drosophila* were placed on ice for sedation, and then placed in a well plate containing the dissection buffer. Under a dissection microscope the head and abdomen were removed with forceps. The legs were then separated from the thorax with forceps, and an incision was made medial to the thorax. The indirect flight muscle was visible as opaque, white tissue. The exoskeleton, intestines, and additional debris were separated from the muscle with a needle. The dissection buffer and muscle were then transferred via micropipette to a 1.5 mL Eppendorf tube. The solution was agitated by aspiration with a pipette until the white muscle was no longer visible. At this point the muscle had been separated into myofibrils.

In a fume hood 43µL of formaldehyde was added to the myofibril solution to create a 4% formaldehyde solution. Tap water was added to fill the tube to the 0.4mL mark. The solution was stirred on a shaker table for one hour. After fixing, the solution was centrifuged for two minutes at 3000 rpm to allow the myofibrils to settle out of solution, and the aqueous formaldehyde

supernatant was pipetted off. The tube was filled to the 0.4mL mark with tap water and aspirated via pipette until transparent. The mixture was stirred on a shaker table for five minutes, and then centrifuged for an additional two minutes. This rinsing procedure was repeated one additional time.

The myofibrils were mounted in water on VWR 22×50 mm microscope cover glass with a Parafilm spacer. An 18×18mm VWR micro cover glass was sealed with Sally Hansen Xtreme Wear Clear nail polish and allowed to dry overnight. Dry samples were prepared by pipetting onto VWR 22x50 mm microscope cover glass and allowing the water to evaporate overnight in a temperature-controlled laboratory at 21˚ C. A coverslip was not used for dry samples. After preparation, the samples were imaged within five days.

2.2 Myofibril Identification

To mark the location of identified myofibrils, high-resolution brightfield microscopy was performed using an Olympus CH-2 Brightfield microscope with a 4x objective lens. Viewing was performed with a digital camera connected to the microscope and computer, so that photos of myofibril location could be captured. The resulting image was 2868 μm × 2149 μm. White light images were captured using AmScope 3.7 software. After myofibril identification, the location was marked with a permanent marker (Figure 8).

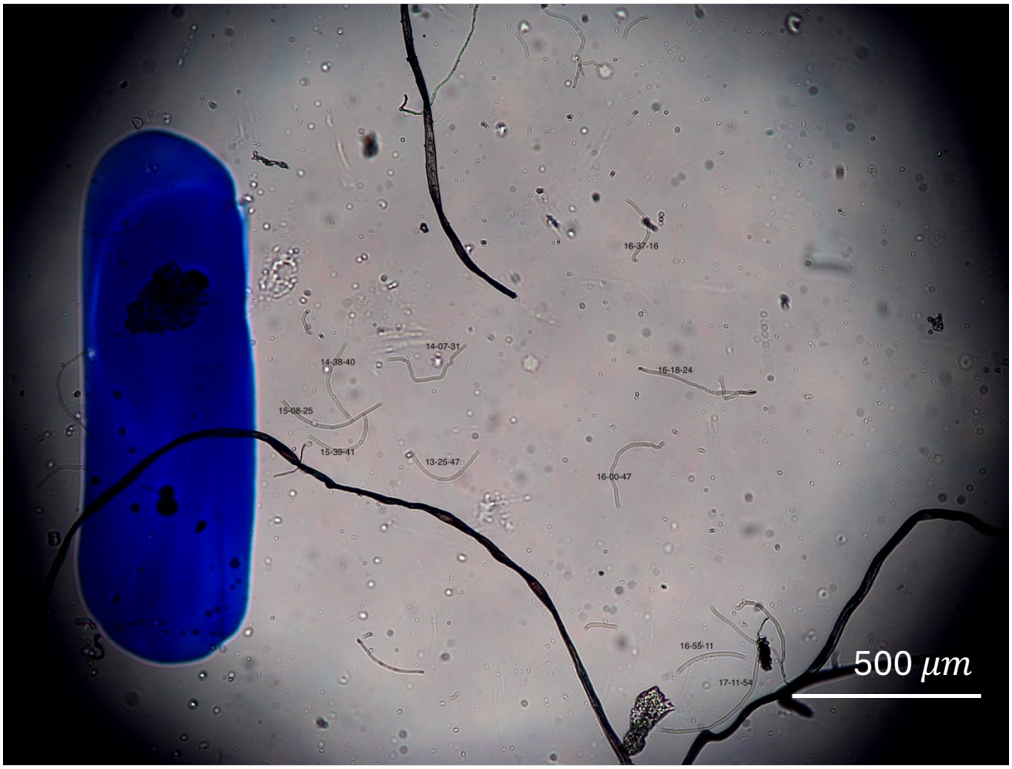

Figure 8: A brightfield microscopy image of a microscope slide containing individual myofibrils. On the left a blue marker spot was drawn for landmark identification. Individual myofibrils can be seen to the right of this spot, with numbers corresponding to the corresponding PIPO scan file. The larger dark lines are likely pieces of muscle that were not fully differentiated into myofibrils.

The slide was then transferred to a custom-built PIPO SHG microscope. A digital camera was paired to the microscope, with the marker dot placed over the objective. The microscope stage was moved according to the built-in coordinate system of the SHG microscope stage (SHG coordinates). Through referencing the brightfield images, the slide was moved to find the myofibril based on its location with respect to the marker dot. This brought the myofibril into the correct location for SHG microscopy.

2.3 PIPO SHG Microscopy

The following PIPO SHG microscopy protocol was performed in a Class 4 Laser Laboratory at Saint Mary's University, Halifax, NS. The ρ values reported in this study are

obtained using a custom-built polarization-in polarization-out (PIPO) SHG microscope. A simplified schematic of this microscope is shown in Figure 9. SHG was generated by a FemtoLux 3 laser from Ekspla. The wavelength of the laser was 1030 nanometers (nm), and the pulse rate was 5 megahertz (MHz). Each pulse lasted 290 femtoseconds (fs). The laser power used was between 5-10mW.

This linearly polarized laser beam was passed through a polarization state generator (PSG), consisting of a LPVIS100 (Thorlabs Inc.) stationary linear polarizer, to polarize the beam. The beam was also passed through a rotating half-wave plate in a motorized mount (WPMP2-22-V1030, Karl Lambrecht Corp.), which allowed the incident laser beam to be rotated. The beam was then focused to the sample with a 0.8 numerical aperture (NA) Plan-Apochromat 20x excitation objective (EO) from Carl Zeiss AG.

The microscope slide was mounted on a motorized stage, and myofibrils were moved to the correct location as described in Section 3.2. The laser beam was then scanned across the focal region using ScannerMAX galvanometric scan mirrors (Pangolin Laser Systems Inc.). The beam was moved row by row in a zig-zag pattern from top to bottom, in a technique known as raster scanning.

The SHG generated at each pixel was then collected by a 0.85 numerical aperture collection objective from Omex Technologies in the forward direction. The polarization of the SHG signal was measured by a polarizing filter (LPVISA 100, Thorlabs Inc.) in a rotating mechanical mount. This is referred to as the polarization state analyzer (PSA). An interference filter (65-253 Edmund Optics) filters the SHG signal at 515nm and a bandwidth of 10nm, eliminating the laser and

potential fluorescence signals. A photomultiplier tube (PMT) then detects the SHG signal via photon counting.

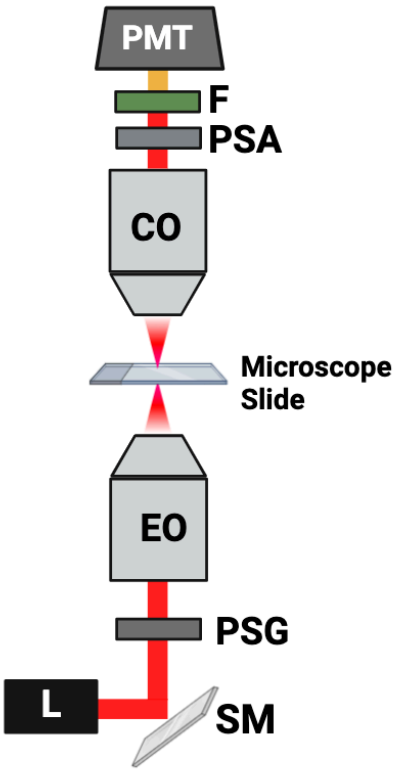

Figure 9: A simplified schematic of the custom-built SHG microscope. Abbreviations: L-laser, SM-scanning mirror, PSG- polarization state generator, EO-excitation objective, CO-collection objective, PSA-polarization state analyzer, F-filter, PMT-photomultiplier tube. Figure was created in BioRender.

The PSG and PSA are each varied to eight angles, giving 64 combinations. At each polarization combination, an intensity image is obtained by summing 50 individual frames, each with 100 × 100 pixels and 18 × 18 μm size. A 65th image is also obtained at the same PSG and PSA angles as the first image to determine sample movement and the average of the SHG intensity at each pixel. Each PIPO SHG scan lasted around 20 minutes.

2.4 Data Fitting

The SHG intensity image was analyzed using ImageJ (v 1,53t, National Institute of Health), an image processing program, where all 64 images can be viewed. A line profile was drawn across the diameter of the myofibril at the initial polarization, and the resulting SHG intensity was plotted. This was repeated at the final polarization, and the initial and final SHG intensity were compared to determine if the sample burned. A decrease in SHG intensity of greater than 10% between the initial and final polarization was considered burning, and these scans were not used for further analysis. If the fibril visibly changed position, the scan was also discarded for movement. These steps ensure that there was no photodamage or movement that would alter the intensity of the SHG signals during scanning.

The SHG intensity image was then analyzed using a custom MATLAB program, where the 65 polarization images were stacked to generate one average intensity image. Using this program, a test for smaller movement was performed by calculating the number of pixels moved between the first and last image. Scans with movement greater than one pixel were discarded.

Determination of ρ values assumed that individual myofibrils possess cylindrical hexagonal (C_{6v}) symmetry. The custom-built optical microscope contains a Cartesian coordinate system (XYZ) in which the laser beam propagates along the Y axis and the myofibril lies in the XZ plane. This coordinate system is shown in Figure 10, where δ represents the orientation of the myofibril with respect to the Z-axis, and α represents the orientation angle out of the XZ plane. From the intensity image, the AP offset, which is the difference in angle between the analyzer and polarizer, was determined.

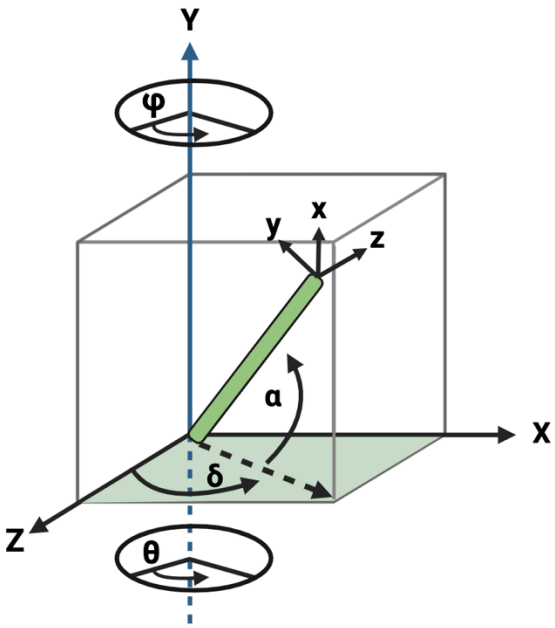

Figure 10: The laboratory XYZ coordinate system of the non-linear optical microscope. The image plane is in the XZ quadrant. The laser beam propagates along the Y axis. The blue line represents a myofibril. δ represents the orientation of the myofibril with respect to the Z-axis, and α represents the orientation angle out of the XZ plane. This diagram was created in BioRender.

The intensity at each pixel was then correlated to ρ through Equation 3. The ρ value is a non-linear optical susceptibility tensor component ratio that is related to the level of disorder in a sample based on variation in helical pitch. I_{SHG} represents the SHG intensity, θ represents the laser electric field linear polarization orientation, and φ represents the orientation of the PSA analyzer. δ is the orientation of the myofibril with respect to the Z-axis.

$$I_{SHG} \propto |\sin(\varphi-\delta)\, sin2(\theta-\delta) + \cos(\varphi-\delta)\sin^2(\theta-\delta) + \rho\cos(\varphi-\delta)\cos(\theta-\delta)|^2 \quad (3)$$

The ρ value at each pixel was determined through correlating intensity to ρ using Equation 3. The SHG intensity image was then shown as a contour plot showing ρ at each pixel on a colour scale. R^2 was calculated in this program, and only pixels with an R^2 value greater than 0.8 were

considered for further analysis. The ρ value at each pixel was determined by a contour plot. An example of a contour plot, or PIPO bubble, can be seen in Figure 7. The average ρ value for the entire fibril was determined by fitting an occurrence histogram of ρ at each pixel to a Gaussian function. The centre position of the Gaussian function represents the mean value. This analysis was carried out in the custom MATLAB program written by Dr. Richard Cisek in the Tokarz Lab.

2.5 Data Analysis

2.5.1 Sarcomere Measurement

Sarcomere lengths were measured from SHG data using ImageJ software. To measure sarcomere length, a segmented one-pixel width line was manually drawn medially across the myofibril. A spline fit was then applied. A line profile was generated, and plotted in ImageJ so that for each sarcomere an intensity curve was obtained. An example of an intensity curve from a myofibril is shown in Figure 11. The data was analyzed in a custom peak-fitting program written for the TokarzLab in LabVIEW 2019. In this program the generated plot was flipped, and the peak of each intensity profile was manually selected, and subsequently all the peaks were automatically fitted with Gaussian curves. The centre locations of the Gaussians were subtracted to give the length between dips in intensity, which corresponded to the Z-line sarcomere measurements.

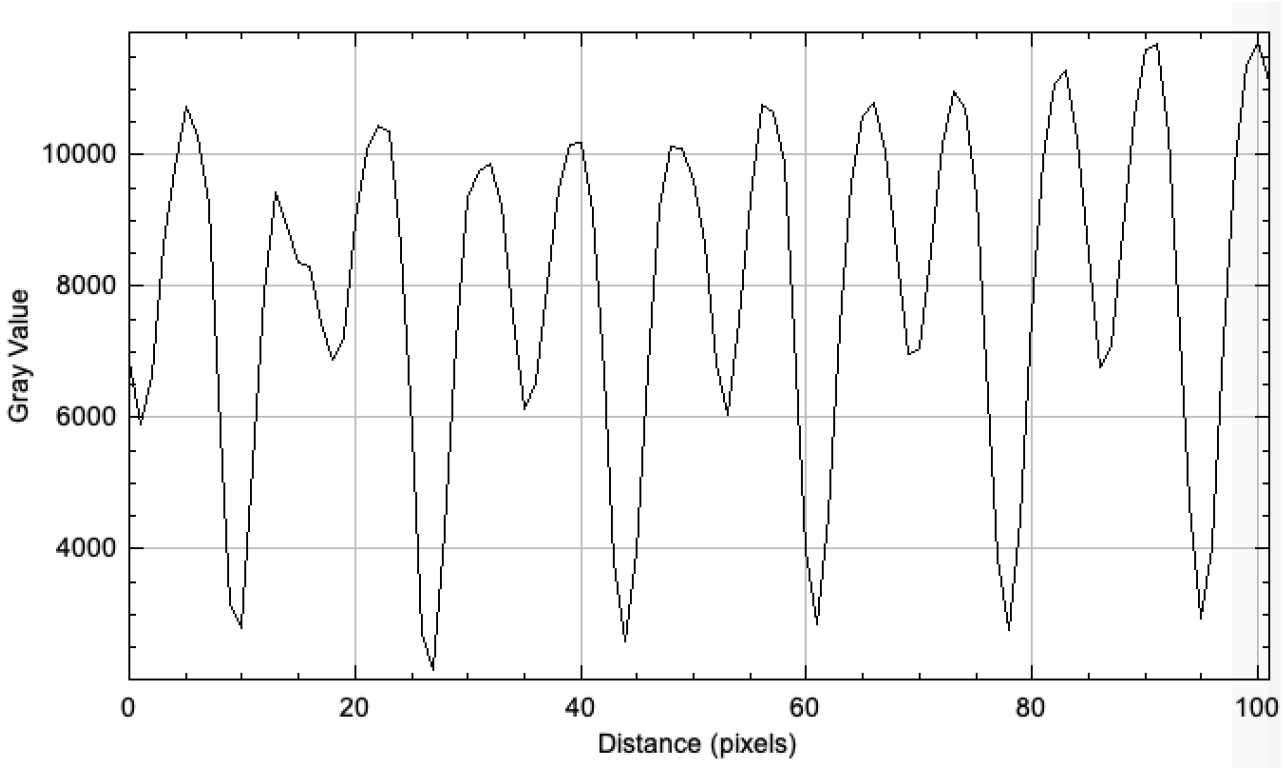

Figure 11: An intensity curve generated from a manually drawn line profile medial to a myofibril in ImageJ. Each curve corresponds to a single sarcomere, and the dip in the center of each peak represents the M-line. The minimum intensity values (shown as "Gray Value" on the Y-axis) correspond to the Z-lines, which have a low concentration of SHG emitters.

2.5.2 Diameter Measurement

Myofibril diameter measurements were obtained using ImageJ. A one-pixel thick line profile was drawn perpendicular across the myofibril from an average SHG intensity image from a PIPO scan, and a line profile was plotted. The data from this plot was copied into MATLAB and fit to a Gaussian. The Gaussian width was converted to a full width half maximum, and used as a diameter measurement, as validated by high resolution microscopy (see the following section).

2.5.3 Atomic Force Microscopy

To validate the accuracy of measurements obtained from SHG intensity images, atomic force microscopy (AFM) was performed for comparison. AFM was performed in the laboratory of Dr. Laurent Kreplak at Dalhousie University. This technique involves tapping a small cantilever tip across a sample to measure the height of the material. Peak force tapping mode was used with a 2nm tip and 25nN of force. The high resolution of AFM allows for extremely accurate myofibril measurements. The fibrils imaged with AFM were also imaged with SHG intensity, and the sarcomere length and diameter measurements were taken from both methods for comparison.

3.0 Results and Discussion

3.1 SHG Intensity and PIPO Imaging of Wet, Relaxed Myofibrils

PIPO SHG intensity scans were performed using the custom-built microscope described in Section 2.3 to determine if individual myofibrils can be successfully imaged using this technique. Figure 12 shows an SHG intensity image of a myofibril in water. Each intensity image is 18 μm × 18 μm and 100 × 100 pixels. Brighter pixels indicate greater intensity of SHG emission.

Individual sarcomeres can be characterized by the banding pattern of light and dark regions. Based on a previous study showing that myosin is the SHG emitter in myofibrils, regions of the sarcomere can be identified using the intensity image. The bright regions correspond to the A-band where myosin is present. In the middle of the A-band a decrease in signal can be seen, which corresponds to the M-line. The dark regions represent the I-band, which is composed of non-SHG emitting actin.

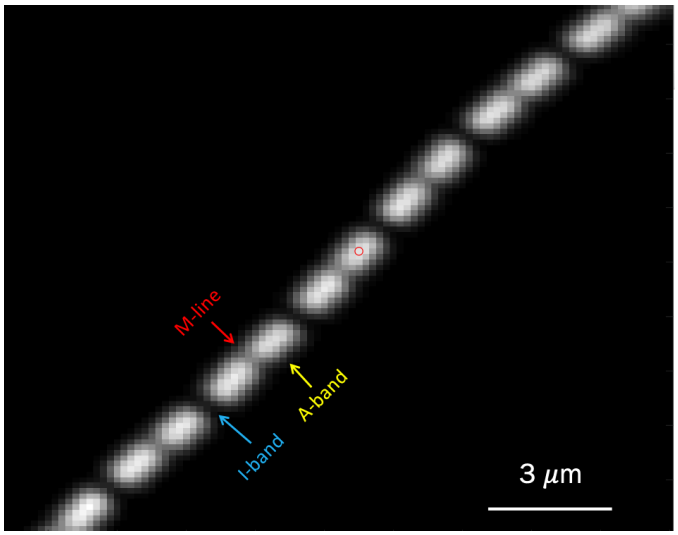

Figure 12: A stacked image of all PIPO SHG intensity scans of an individual relaxed myofibril. SHG intensity is represented by a colour scale with black being the lowest intensity and white being the most intense. The myofibril was dissected in ATP and imaged in water using PIPO SHG microscopy.

The PIPO SHG intensity images were then fit to Equation 3 to determine the ρ value at each pixel. This was performed using a custom-designed program in MATLAB. A ρ image is then generated with a colour corresponding to ρ at each pixel, with red pixels indicating a greater ρ value and blue indicating a lower value. This colour mapping scale is shown by the colour bar in Figure 13. Greater ρ values were associated with a greater degree of disorder in the helical pitch.

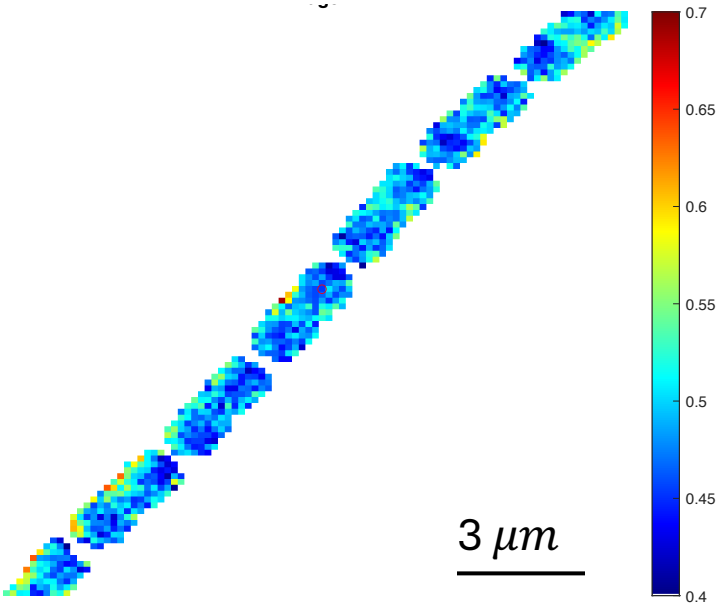

Figure 13: A colour map showing the ρ value at each pixel of the same myofibril shown in Figure 18. This myofibril was imaged by PIPO SHG microscopy and fit using a custom program in MATLAB. The myofibril was dissected in ATP and imaged in water using PIPO SHG microscopy.

The results of the SHG intensity imaging shows that individual myofibrils can be successfully imaged using the custom-built PIPO microscope. Figure 14 shows a typical occurrence histogram of the ρ value at each pixel. Fitting this histogram to a Gaussian allowed the mean ρ value for the entire fibril to be calculated. Averaging the mean ρ value for entire myofibrils from 60 images showed that individual myofibrils in water have a mean ρ value of 0.544 ± 0.03, where the uncertainty is the standard deviation.

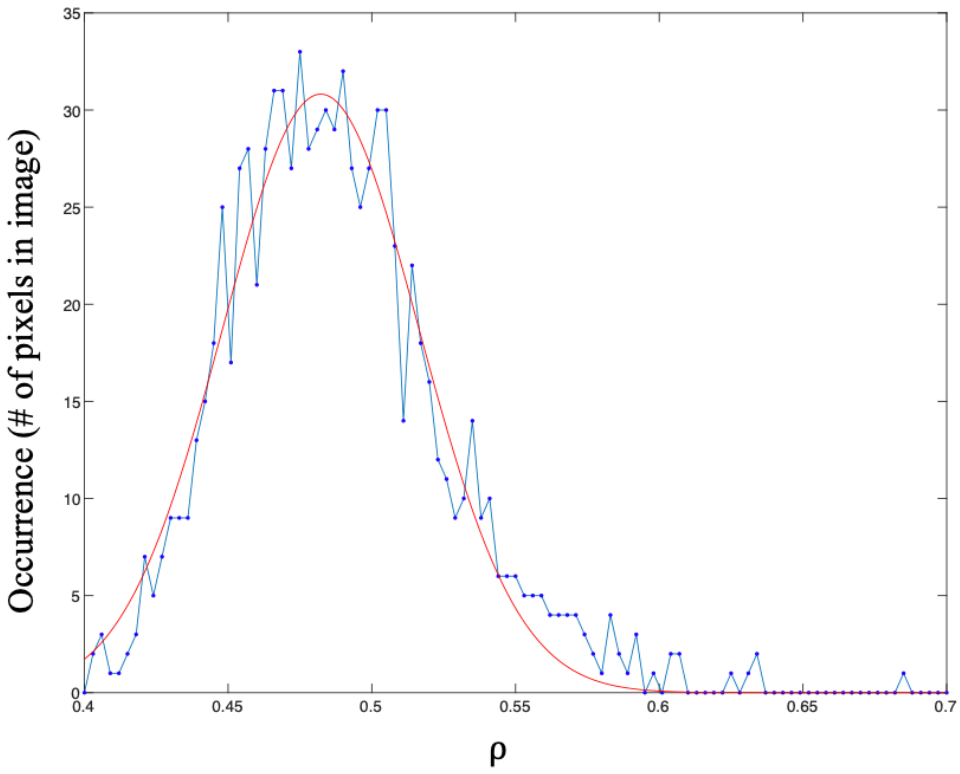

Figure 14: An occurrence histogram of the ρ values displayed in Figure 13. Using a custom program in MATLAB this histogram was fit to a Gaussian, and the middle number represents the average. The blue curve shows the collected occurrence data, and the red line shows the Gaussian function.

3.1.1 Three Populations of Wet, Relaxed Myofibrils

Scans of relaxed myofibrils in water revealed three populations of myofibrils. The first showed a mean ρ value of slightly below the wet, relaxed myofibril average of 0.544 ± 0.03, and little variation in ρ throughout the fibril. Among the three populations of fibrils, all fibrils had uniformity in ρ values in the direction of the fibrils. An example of this population can be seen in Figure 13. The second population had a gradient in ρ values across the fibril, resulting in a wider histogram, as shown in Figure 15. The gradient has been previously observed in individual

collagen fibrils.[21] This can be explained by the non-uniformity of the focal field due to the high numerical aperture.[21]

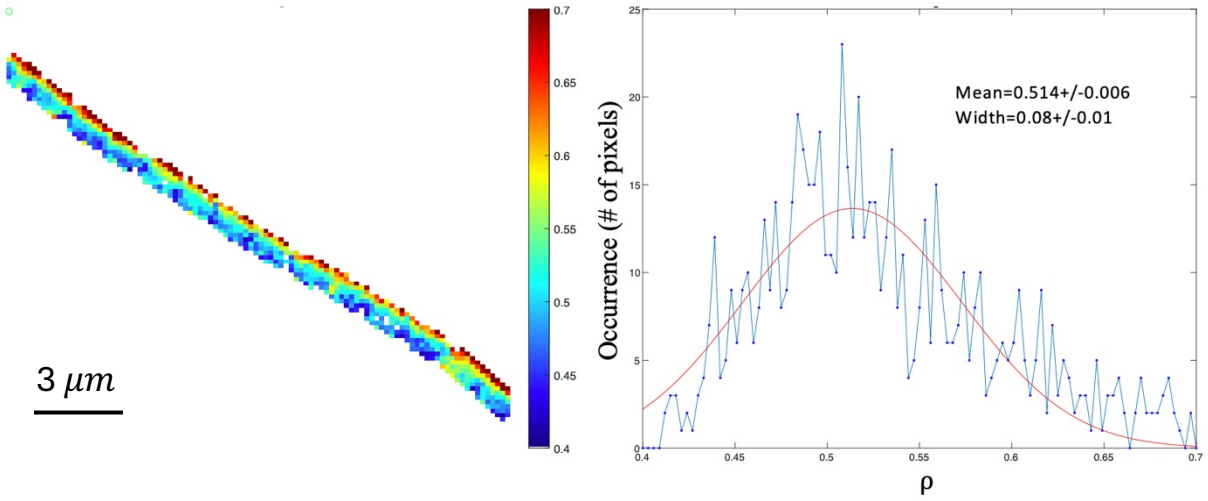

Figure 15: The left image is an example of a myofibril with a gradient in ρ value perpendicular to the direction of the fibril. The myofibril was dissected in ATP and imaged in water using PIPO SHG microscopy. The right is an occurrence histogram of the ρ values from the left image.

The third population of wet, relaxed myofibrils had a higher mean ρ value per fibril than the overall average. Many of the fibrils in this third population also had higher ρ values on both edges of the fibril, as seen in Figure 16. As ρ is proportional to the amount of disorder in a sample, the higher mean ρ value in these myofibrils can be attributed to damage. This damage may have resulted from the dissection procedure, or from burning with the laser. The presumed damaged fibrils were disregarded in future experiments.

Damage sites can also be observed at kinks of fibrils. As shown in Figure 17, bent regions of myofibrils have a much higher ρ ratio, attributed to local damage, and hence increased level of disorder at the kink.

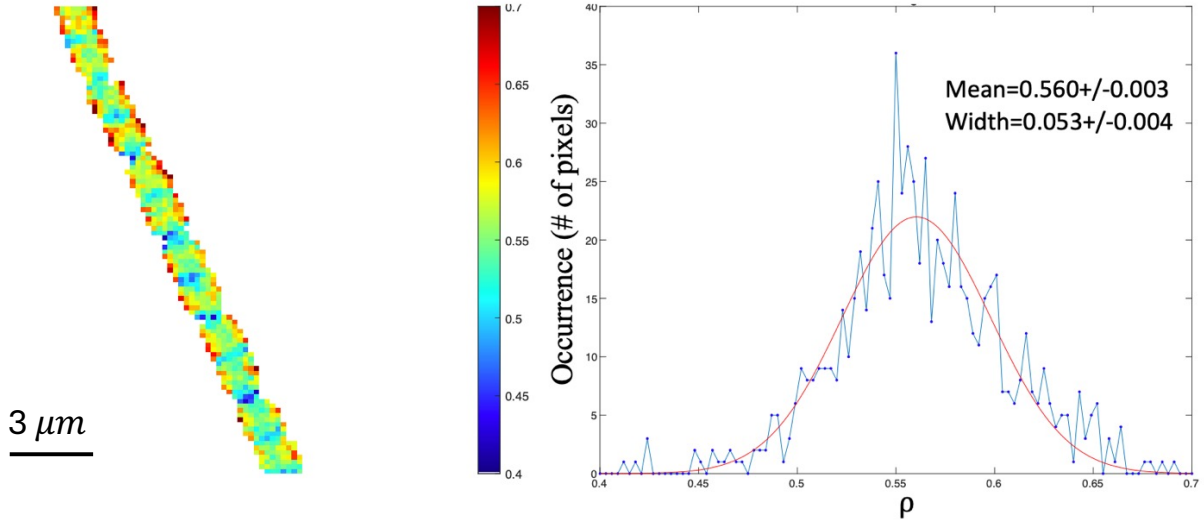

Figure 16: The left image shows an example of a presumed damaged myofibril. The myofibril was dissected in ATP and imaged in water using PIPO SHG microscopy. The right image shows an occurrence histogram, and higher ρ ratio of this population of fibrils.

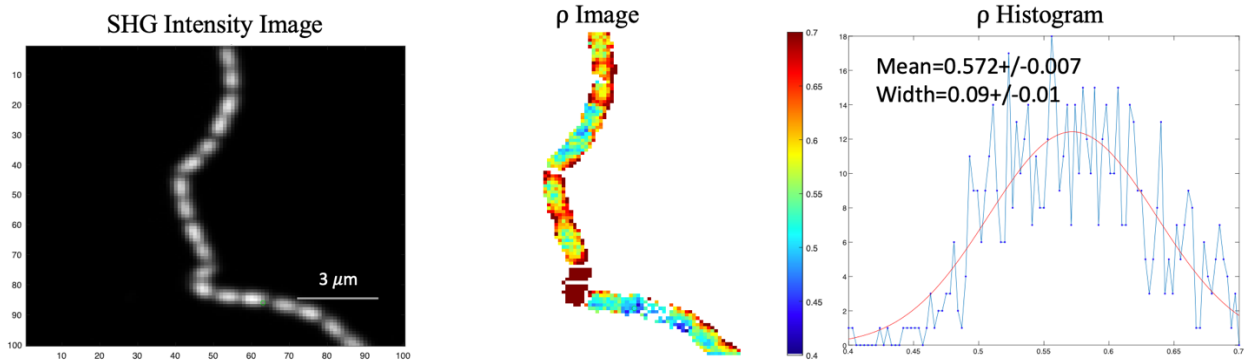

Figure 17: The left image is an SHG intensity image of a kinked fibril. The center image shows the colour map of ρ values at each pixel. The higher ρ values can be observed in the kinked region. The right image shows an occurrence histogram from the ρ values of this fibril. The myofibril was dissected in ATP and imaged in water using PIPO SHG microscopy.

3.1.2 Gradient in ρ Values

A gradient in ρ values was observed in twelve myofibrils. A gradient across individual collagen fibrils has been previously reported.[21] The gradient results from the use of a high numerical aperture objective, which generates circular polarization at the edges of the focal

volume.[21] The SHG intensity at the edges of the myofibril therefore have a longitudinal component from the incoming circular polarization.[21] This circular polarization has an opposite direction on each side of the fibril. The longitudinal electric field contributes to the SHG intensity. Due to non-uniformity in the focal field, the contribution of the longitudinal component of the electric field to the SHG intensity will vary across the fibril.[21] Because SHG intensity is related to ρ, this creates a gradient longitudinal to the fibril.

When collagen fibrils were rotated 180˚, the gradient remained in the same direction. This indicates that the origin of SHG in collagen fibrils is not from electric-dipole effects.[21]. Simulations have shown that the gradient will flip if it results from only electric-dipole effects, meaning that SHG intensity relies only on the $\chi^{(2)}$ tensor and the electric field of the laser light.[21] This electric field creates a dipole by generating movement in the electrons in the sample, which causes SHG. However, if the gradient does not flip with rotation, the gradient may result from $\chi^{(2)}$ tensor, the electric field of the laser light, and the magnetic field of the laser light.[21]

Rotation experiments were performed on myofibrils to test if the gradient in muscle results from electric-dipole effects. It was found that the gradient changed orientation with the fibril (meaning the gradient flipped), and examples of the gradient flipping are shown in Figure 18. This indicated that the SHG in myofibrils may occur due to an electric-dipole resonant interaction, unlike collagen.

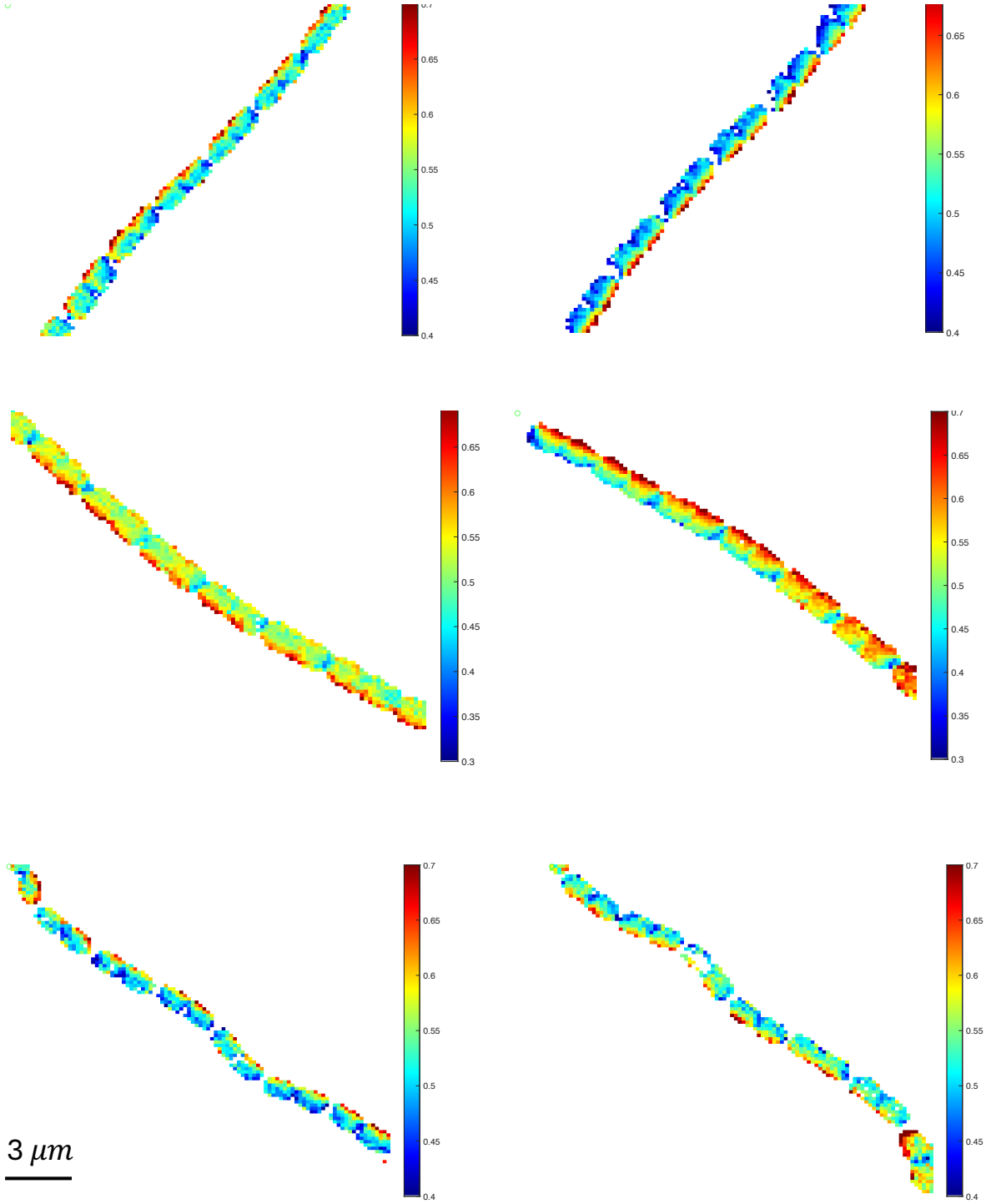

Figure 18: Three examples of a gradient in ρ across individual myofibrils. The images on the left show the fibril before rotation, and the corresponding image to the right shows the same fibril after 180˚ rotation of the microscope slide. Unlike in collagen, the gradient is shown to change direction when the fibril is rotated.

The gradient of two myofibrils, out of 12 that showed a gradient, were found not to flip with rotation. The reason for this is unknown but may be attributed to burning. The investigation of why these gradients did not flip with rotation is a direction for future work.

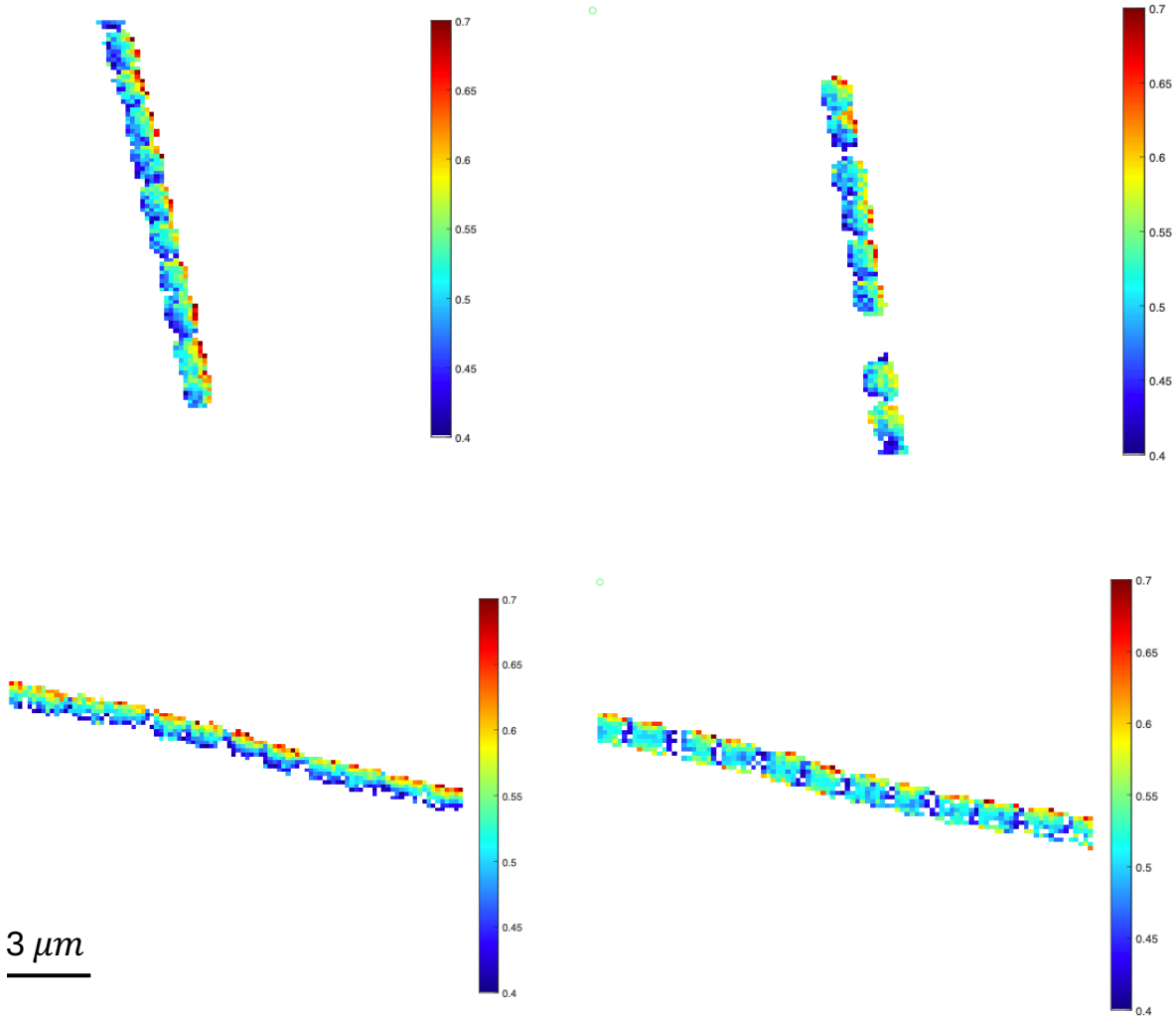

Figure 19: Two examples of a gradient in ρ across individual myofibrils (shown in the left images). The corresponding image to the right shows the same fibril after 180˚ rotation of the microscope slide. Unlike in other myofibrils image, the gradient in these two fibrils did not change direction when the fibril was rotated.

3.2 SHG Intensity and PIPO Imaging of Dry, Relaxed Myofibrils

SHG intensity images and PIPO scans were also obtained of dry, relaxed myofibrils. The mean ρ value for whole, dry myofibrils was found to be 0.45 ± 0.02, where the uncertainty is the standard deviation.

An SHG intensity comparison of wet and dry myofibrils was performed through imaging with circularly polarized light. The results of this study are shown in Figure 20. This was achieved through use of a quarter wave plate in the path of the laser beam. The use of circularly polarized light allows for an orientation-independent comparison of SHG intensity. The results of this comparison show that wet myofibrils have a higher SHG intensity than dry myofibrils imaged at the same laser power. SHG intensity is proportional to the concentration of SHG emitters squared, and so these results suggest that myofibrils in the hydrated state contain more SHG emitters.

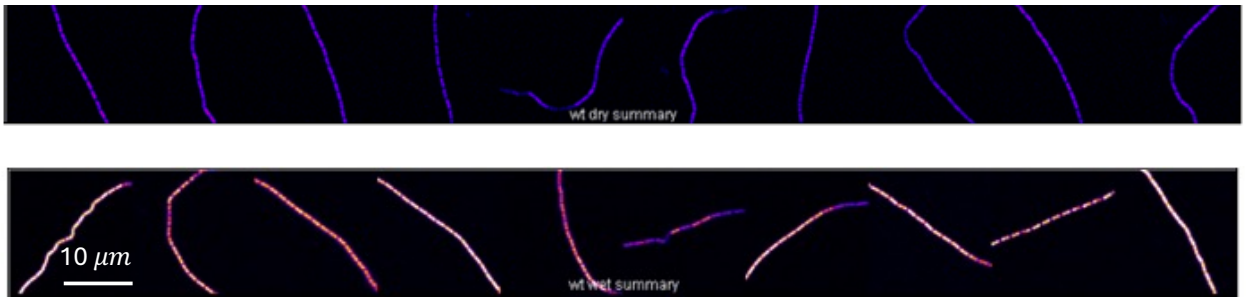

Figure 20: SHG intensity images of ten dry myofibrils (top row) and ten wet (bottom row). The SHG intensity is shown by colour, ranging from low intensity shown as purple and high intensity shown as white.

3.3 Relationship Between Sarcomere Length and ρ

3.3.1 Confirmation of Measurement Methodology

To measure sarcomere length from the SHG intensity images, a custom Gaussian fitting program was used in LabView 2019. Extrapolating a line profile from an SHG intensity of a myofibril generates a Gaussian-shaped curve for each sarcomere due to the decrease in intensity at each I-band. To test the accuracy of this method, atomic force microscopy (AFM) measurements

were taken for measurement comparison. In AFM peak-force tapping mode, a small tip is tapped along a surface to measure the height of a sample. Due to the small tip size, AFM images have high resolution, allowing for accurate length and diameter measurements.

SHG intensity images and AFM sarcomere length and diameter measurements were taken of the same fibrils. The AFM measurements are shown in Figure 21. A comparison of the SHG and AFM measurements (shown in Figure 22) found the measurements from the SHG intensity images to be accurate within 10%. After confirming the accuracy of the SHG intensity measurements this technique was used for all measurements due to the expense and time consumption of AFM.

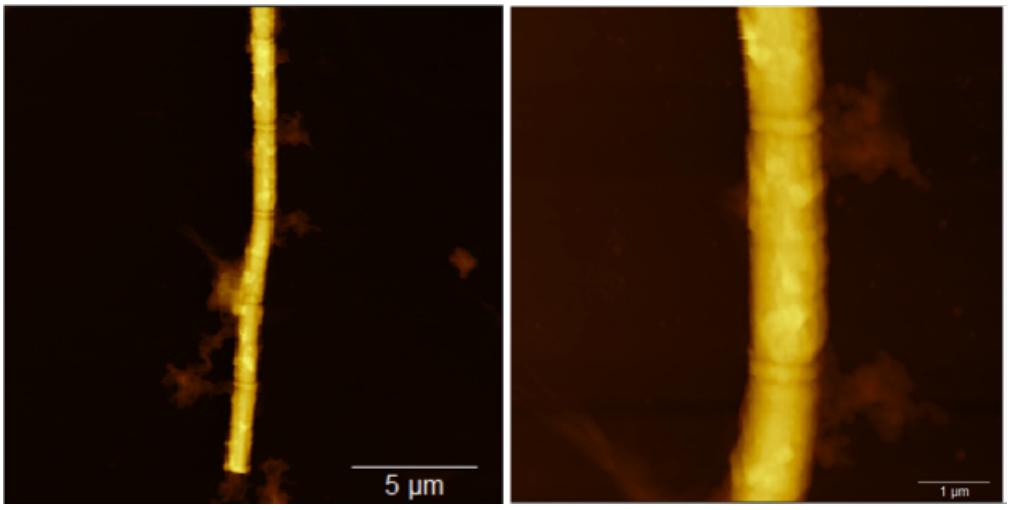

Figure 21: Atomic force microscopy (AFM) images of dry myofibrils. These images were collected in the lab of Dr. Laurent Kreplak at Dalhousie University.

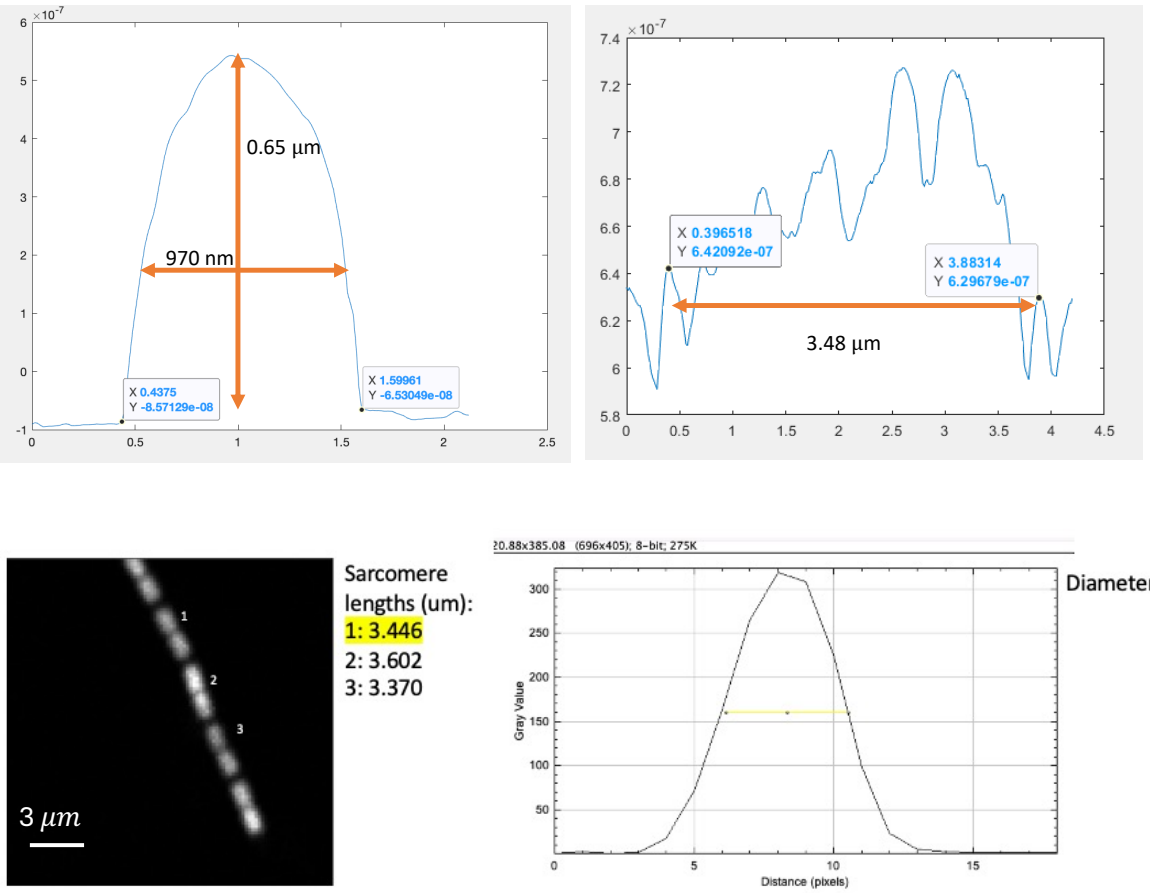

Figure 22: Diameter and sarcomere length measurements of the same fibril from AFM images (top) and SHG intensity images (bottom). SHG sarcomere length measurements were taken using a Gaussian fitter.

3.3.2 Relationship Between Sarcomere Length and ρ

Sarcomere length measurements and corresponding mean ρ values were taken from over 200 sarcomeres to determine if there is a relationship between sarcomere length and ρ. Average ρ was taken from the middle three pixels of each sarcomere with three pixels omitted on each sarcomere end. This was done to avoid the falsely increased ρ values at the edges caused by the gradient effect.

Based on previous study, it was hypothesized that ρ will increase as sarcomere length decreases due to an increase in molecular disorder with contraction. Figure 23 shows that in wet,

relaxed myofibrils there is no relationship between sarcomere length and average ρ value. This is consistent with the findings of Nucciotti et al., who found no relationship when myofibrils were in the relaxed state.[8]

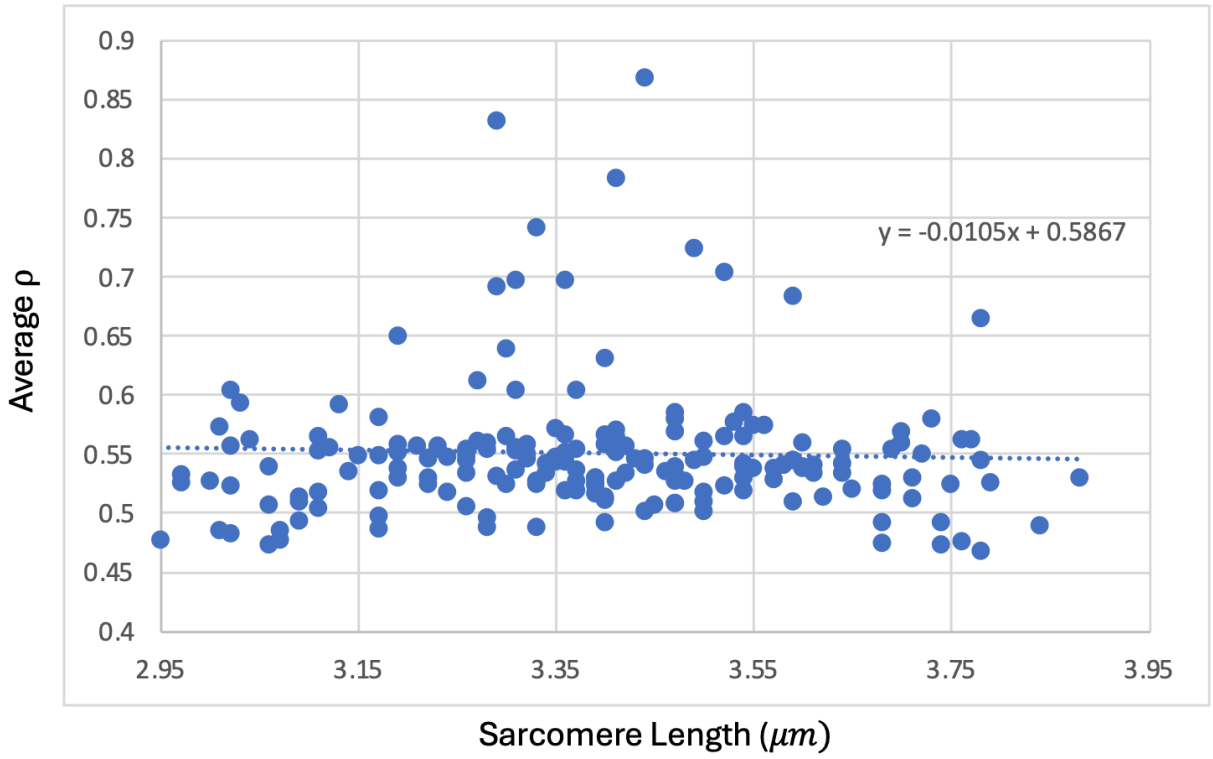

Figure 23: A plot of average ρ vs sarcomere length for wet, relaxed myofibrils.

To simulate rigor mortis, myofibrils were dissected in a lower concentration of ATP to induce contraction. One batch of fibrils were dissected in half the amount of ATP as the relaxed state, and another in no ATP. The fibrils were then fixed and imaged to determine sarcomere length and mean ρ at the middle three pixels of the fibril. Within the 0.5x ATP myofibrils there is a negative correlation between sarcomere length and mean ρ value (Figure 24).

The myofibrils dissected in 0x ATP were difficult to isolate. There were significantly less fibrils deposited on the slide, and they burned easier when scanned. Because of this sarcomere length and mean ρ were collected from only two fibrils. In the 0x ATP population there was a slightly positive correlation between the sarcomere length and ρ (Figure 32), although due to the small sample size more study is required to draw conclusions from this data alone.

When the data from both the 0.5x and 0x ATP populations are combined in a graph, there is a negative correlation between sarcomere length and ρ (Figure 33). This is agreeance with the findings of Nucciotti et al., who found that the ρ ratio increases as sarcomere length decreases in fibrils in the *rigor* state.[8] This comparison can be made with our pooled 0.5x and 0x ATP data, as it presumed that the fibrils in both populations are in some form of *rigor* due to ATP deprivation.

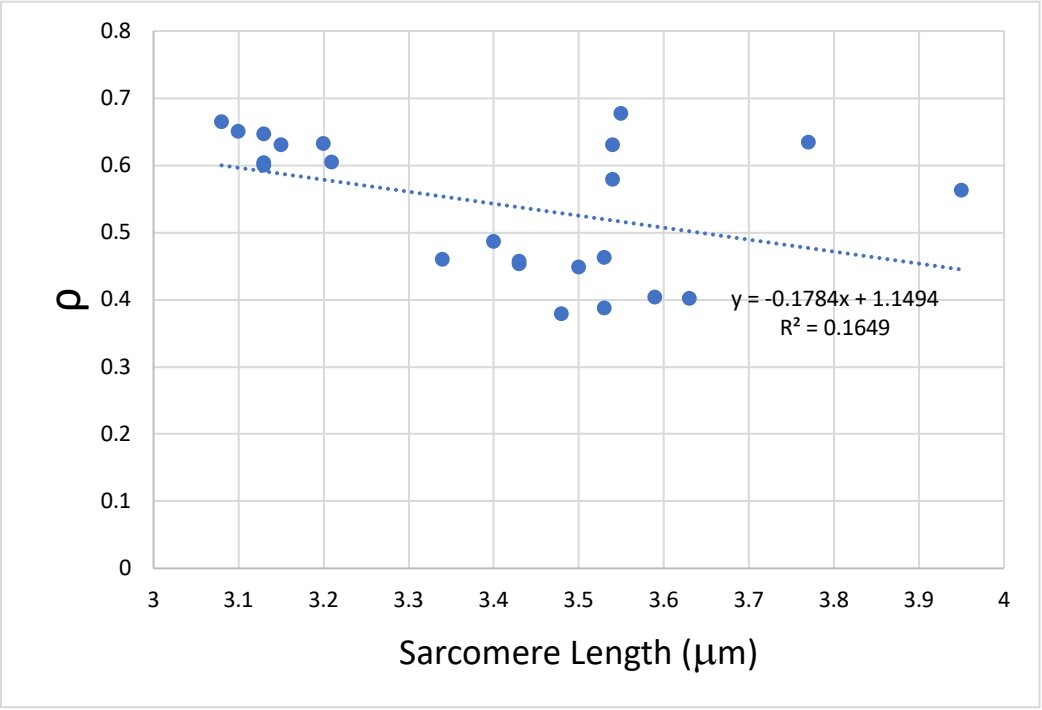

Figure 24: Sarcomere length vs ρ for myofibrils dissected in 0.5x ATP.

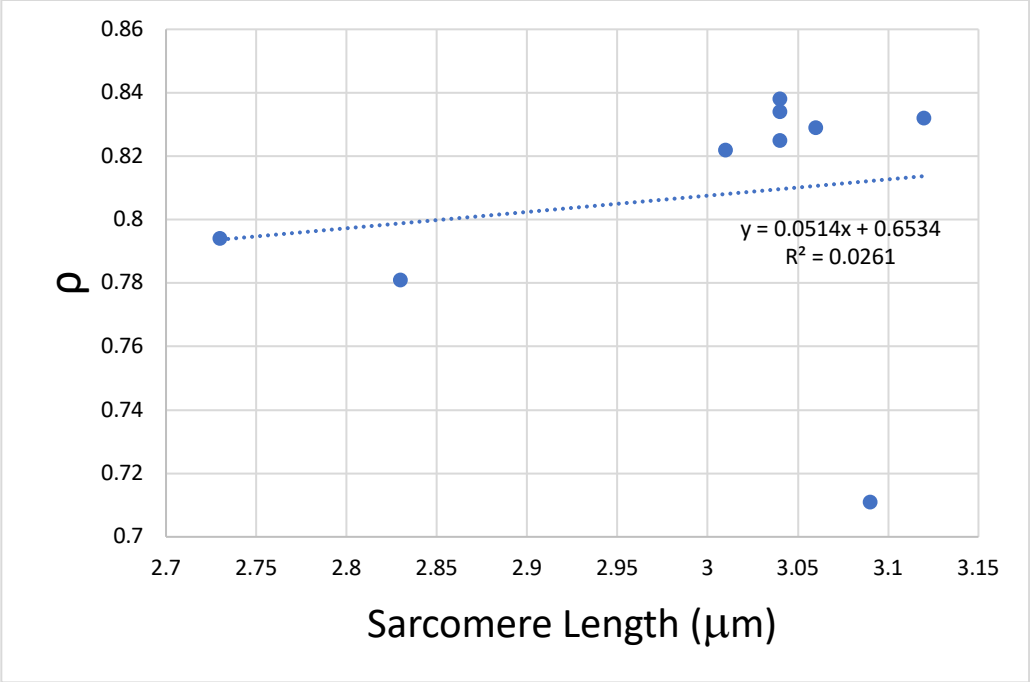

Figure 25: Sarcomere length vs ρ for myofibrils dissected in 0x ATP.

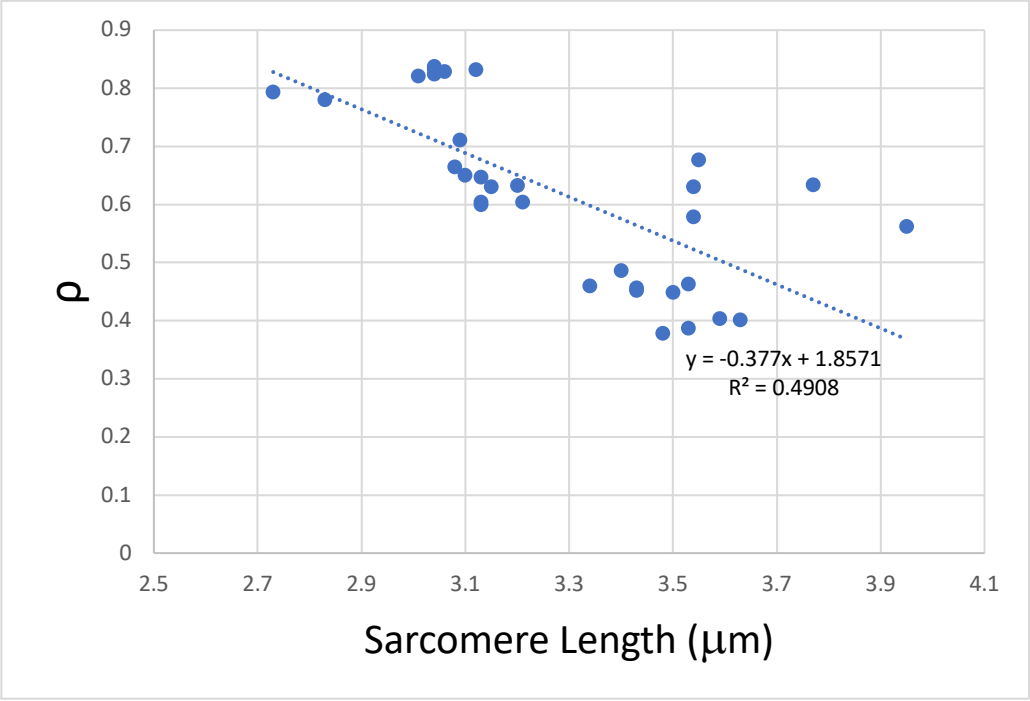

Figure 26: Plot of sarcomere length vs ρ containing data from both myofibrils dissected in 0.5x ATP and 0x ATP.

3.4 ρ in Different Regions of a Sarcomere

3.4.1 Relaxed Myofibrils

Myofibrils dissected in a physiological concentration of ATP and imaged in water were analyzed to observe variation in ρ values in different regions of the sarcomere. Myofibrils with an average ρ value above 0.6, which are presumed to be damaged or burned, were excluded from this analysis. The average ρ value in the I-bands of this population of myofibrils was 0.44 ± 0.04. The average ρ value in the A-bands of these myofibrils was 0.52 ± 0.01. This was found by averaging the middle three pixels of the A-band on each side of the M-line, as shown in Figure 27. The average ρ value in the M-line was found to be 0.47 ± 0.06. The uncertainty of averages presented is the standard deviation. A two-tailed paired sample t-test was performed to determine if there was a significant difference in the mean ρ value in the three analyzed regions of the sarcomere. It was found that in the relaxed state the A-band has a significantly higher mean ρ value than the M-line and I-band. The average ρ value in the M-line and I-band was not significantly different.

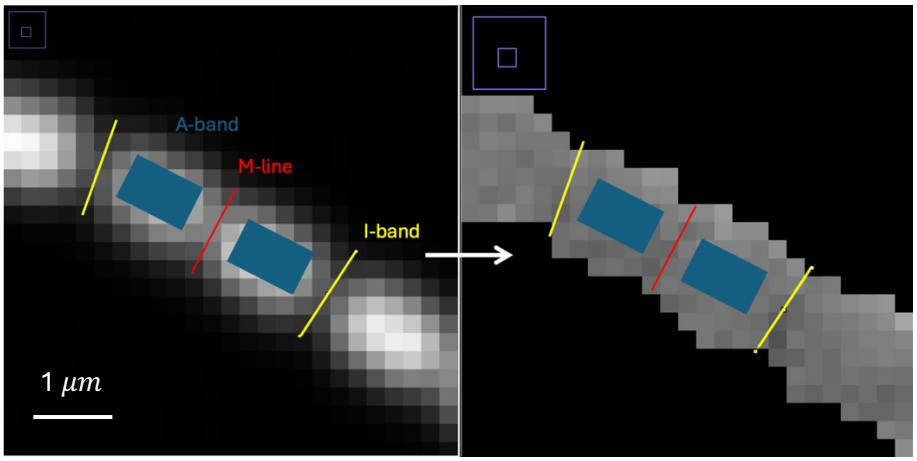

Figure 27: A diagram of the three regions analyzed per sarcomere. The left image shows the intensity image, in which the area of interest was selected, and the right image shows the ρ value at each pixel. The area of interest was transferred to the ρ image, and the values in this area were averaged.

Table 1: Paired sample t-test statistics performed to test for a significant difference in the mean ρ value of the I-band, A-band, and M-line of individual sarcomeres of relaxed myofibrils. The average ρ value is presented as mean ± standard deviation. A P value of less than 0.05 was considered statistically significant.

Sarcomere Region	Sample Size, n	Average ρ value	t value (two-tailed)	P value
I-band	15	0.44 ± 0.04	7.619	0.001
A-band	28	0.52 ± 0.01		
A-band	28	0.52 ± 0.01	3.097	0.002
M-line	14	0.47 ± 0.06		
M-line	14	0.47 ± 0.06	1.573	0.1
I-band	15	0.44 ± 0.04		

Samim et al. have also investigated the average ρ value in these regions of the sarcomere in bulk muscle tissue.[20] That study showed a mean ρ value at the M-line of 0.489 ± 0.001, and a mean ρ value at the edges of the A-band of 0.498 ± 0.001.[20] The I-band had an average ρ value of 0.519 ± 0.001.[20]

Samim et al. analyzed the edges of the A band because the ρ ratio was expected to be different on the edges and middle of the A-band as the myosin heads are located along the periphery of myofilaments.[20] Due to the gradient in ρ value observed in our study, the edges of the A-band were not analyzed as the ρ value is artificially higher at edges of the sarcomere in some scans, as shown in Figure 28. Instead, the central three pixels of the A-band were analyzed to avoid the falsely high ρ values affecting the average.

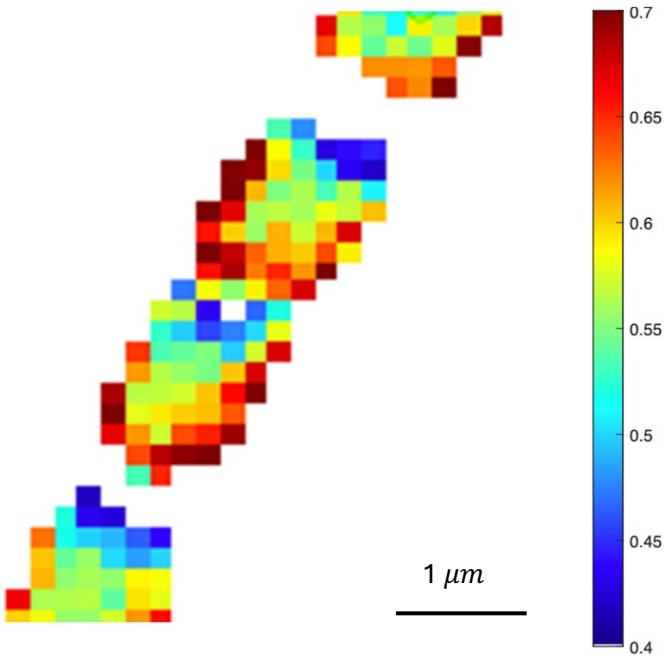

Figure 28: An example of a single sarcomere with a higher ρ value around the edges of the A-band. To avoid skewing of the average ρ value from the gradient produced by a high numerical aperture, only the central pixels were taken from the A-band, as shown in Figure 27.

Samim et al. concluded that their results suggest that the HMM and LMM regions of myosin (shown in Figure 1) have different ρ values.[20] The HMM region contains myosin heads, which increase the level of disorder due to variation in deflection of the heads and in variation in the attached/detached state with actin. Myosin heads are in the A-band of the sarcomere. The M-line is in the central region where the myosin tails meet, and there should be no myosin heads in this region. In muscle tissue the M-line was found to have a lower mean ρ values due to the lack of myosin heads.[20] In individual myofibrils the significantly higher mean ρ value in the A-band may be a result of disorder caused by myosin heads.

Samim et al. found the average ρ values to be ~6% higher in the I-band than the M-line.[20] In our analysis a significant difference was not observed between the average ρ value in the I-band and M-line. This discrepancy may be due to the small sample size analyzed, and if a larger

population is analyzed in future work a significant difference between these regions may emerge. It is also possible that there is a difference in the level of disorder in these regions in muscle tissue compared to myofibrils, which should be investigated in future work.

3.4.2 Non-Relaxed Myofibrils

Myofibrils dissected in 0.5x and 0x the physiological concentration of ATP and imaged in water were analyzed to observe variation in ρ values in different regions of the sarcomere. For myofibrils dissected and fixed in 0.5x physiological ATP, the average ρ value in the I-bands was 0.57 ± 0.07. The average ρ value in the A-bands of these myofibrils was 0.6 ± 0.1. The average ρ value in the M-line was found to be 0.60 ± 0.07.

For myofibrils dissected and fixed in 0x physiological ATP, the average ρ value in the I-bands was 0.79 ± 0.09. The average ρ value in the A-bands of these myofibrils was 0.77 ± 0.07. The average ρ value in the M-line was found to be 0.8 ± 0.2. The uncertainty of averages presented is the standard deviation. In both the 0.5x ATP and 0x ATP population there was found to be no significant difference between the three regions across the sarcomere. Significance was determined by a paired sample t-test, and the results of these tests can be found in Table 2 and Table 3.

Table 2: Paired sample t-test statistics performed to test for a significant difference in the mean ρ value of the I-band, A-band, and M-line of individual sarcomeres of myofibrils dissected in 0.5x ATP. The average ρ value is presented as mean ± standard deviation. A P value of less than 0.05 was considered statistically significant.

Sarcomere Region	Sample Size, n	Average ρ value	t value (two-tailed)	P value
I-band	10	0.57 ± 0.07	0.953	0.3
A-band	20	0.6 ± 0.1		
A-band	20	0.6 ± 0.1	0	1
M-line	10	0.60 ± 0.07		

M-line	10	0.60 ± 0.07	18.207	0.3
I-band	10	0.57 ± 0.07		

Table 3: Paired sample t-test statistics performed to test for a significant difference in the mean ρ value of the I-band, A-band, and M-line of individual sarcomeres of myofibrils dissected in 0x ATP. The average ρ value is presented as mean ± standard deviation. A P value of less than 0.05 was considered statistically significant.

Sarcomere Region	Sample Size, n	Average ρ value	t value (two-tailed)	P value
I-band	18	0.79 ± 0.09	0.397	0.5
A-band	27	0.77 ± 0.07		
A-band	27	0.77 ± 0.07	0.363	1
M-line	14	0.8 ± 0.2		
M-line	14	0.8 ± 0.2	0.174	1
I-band	18	0.79 ± 0.09		

Due to the unstable nature of the myofibrils dissected in 0x ATP, only three successful PIPO scans were obtained for this population. Therefore, the average ρ value in each region from all three ATP concentrations was calculated from only three scans, for a total of 15-25 sarcomeres, despite having significantly more scans of the 1x and 0.5x ATP fibrils. In future work an extensive analysis of the average ρ value of these three regions in relaxed myofibrils should be carried out on the more than 100 myofibril scans collected throughout this project.

3.4.3 Relaxed vs Rigor Myofibrils

Table 4: The average ρ value in three areas of the sarcomere for three ATP concentrations.

ATP Concentration	I-band	A-band	M-line
Muscle Tissue (Samim et al.)	0.519 ± 0.001	0.498 ± 0.001	0.489 ± 0.001
1x	0.44 ± 0.04	0.52 ± 0.01	0.47 ± 0.06
0.5x	0.57 ± 0.07	0.6 ± 0.1	0.60 ± 0.07
0x	0.79 ± 0.09	0.77 ± 0.07	0.8 ± 0.2

The results of the investigation of average ρ value in three areas of the sarcomere for three ATP concentrations are summarized in Table 3. Overall, the mean ρ value in all three regions was found to increase significantly as the ATP concentration decreases. Significance was determined by a paired sample t-test, and the results of this statistical analysis can be found in Table 4. This suggests that contraction increases the level of disorder in all regions of the sarcomere.

Table 5: Paired sample t-test statistics performed to test for a significant difference in the mean ρ value of the same region of myofibrils dissected in different ATP concentrations. The average ρ value is presented as mean ± standard deviation. A P value of less than 0.05 was considered statistically significant.

Sarcomere Region and ATP Concentration	Sample Size, n	Average ρ value	t value (two-tailed)	P value
I-band 1x ATP	15	0.44 ± 0.04	5.322	0.001
I-band 0.5x ATP	10	0.57 ± 0.07		
I-band 0.5x ATP	10	0.57 ± 0.07	7.176	0.001
I-band 0x ATP	18	0.79 ± 0.09		
A-band 1x ATP	28	0.52 ± 0.01	3.564	0.001
A-band 0.5x ATP	20	0.6 ± 0.1		
A-band 0x ATP	27	0.77 ± 0.07	6.895	0.001
A-band 0.5x ATP	20	0.6 ± 0.1		
M-line 1x ATP	14	0.47 ± 0.06	4.756	0.001
M-line 0.5x ATP	10	0.60 ± 0.07		
M-line 0.5x ATP	10	0.60 ± 0.07	3.457	0.002
M-line 0x ATP	14	0.8 ± 0.2		

4.0 Conclusions and Future Work

The results of this study show that individual myofibrils dissected from *Drosophila melanogaster* can be successfully imaged using PIPO SHG. Individual myofibrils dissected and fixed at physiological ATP concentration and imaged in deionized water were found to have a mean ρ value of 0.544 ± 0.03. A gradient in ρ value perpendicular to the direction of the sarcomere was observed in fibrils in this population. The direction of the gradient was found not to flip with rotation of the myofibril, suggesting that SHG in myofibrils may occur due to an electric-dipole resonant interaction. However, the gradient in two myofibrils did flip with rotation. The reason for this is unknown and should be investigated in future work.

An SHG intensity comparison between wet and dry relaxed myofibrils was performed, and the wet myofibrils were found to have a higher SHG intensity. In future work a study of the effects of hydration on SHG intensity in myofibrils should be pursued to explain this result.

The relationship between sarcomere length and ρ value within an individual sarcomere were observed. In the relaxed state no relationship between these variables was observed. In the rigor state, which was induced by dissecting and fixing in 0.5x and 0x the physiological concentration of ATP, the mean ρ value was found to increase as sarcomere length decreased. This suggests that the level of disorder within a sarcomere increases with contraction.

In future work a comparison between myofibrils fixed in different concentrations of ATP with those fixed in a physiological amount of ATP but left to sit for varying time periods before fixing should be investigated. This will provide a better understanding of how *rigor* is induced in individual myofibrils.

Additionally, a decrease in contraction during an ischemic event has been observed to correlate with acidic pHs.[5] In future work myofibrils should be dissected and fixed in varying pHs to expand the understanding on the effects of pH on individual myofibrils during ischemia. A decrease in pH is also observed in *rigor,* and so the relationship between pH, disorder (ρ value), and contraction can be observed.

The average ρ value in the A-band, I-band, and M-line of the sarcomere were observed in both the relaxed and *rigor* state. In relaxed myofibrils the A-band was found to have a significantly higher mean ρ value than the M-line and I-band. This may result from disorder caused by variance in conformation and deflection angle of the myosin heads. The average ρ value of the M-line and I-band was not significantly different, but in future work a greater sample size should be analyzed to confirm this result. In the *rigor* state the mean ρ values of the A-band, I-band, and M-line were not significantly different. Overall, the mean ρ value increased in all three regions as the ATP concentration decreased. This suggests that myosin disorder increased with contraction.

This study demonstrates that PIPO SHG microscopy is an effective tool for measuring myosin disorder. This disorder was found to increase with contraction, and in the future this imaging technique may be applied in the diagnosis of myocardial infarction or ischemia.

5.0 References

(1) Benjamin, E. J.; Virani, S. S.; Callaway, C. W.; Chamberlain, A. M.; Chang, A. R.; Cheng, S.; Chiuve, S. E.; Cushman, M.; Delling, F. N.; Deo, R.; de Ferranti, S. D.; Ferguson, J. F.; Fornage, M.; Gillespie, C.; Isasi, C. R.; Jiménez, M. C.; Jordan, L. C.; Judd, S. E.; Lackland, D.; Lichtman, J. H.; Lisabeth, L.; Liu, S.; Longenecker, C. T.; Lutsey, P. L.; Mackey, J. S.; Matchar, D. B.; Matsushita, K.; Mussolino, M. E.; Nasir, K.; O'Flaherty, M.; Palaniappan, L. P.; Pandey, A.; Pandey, D. K.; Reeves, M. J.; Ritchey, M. D.; Rodriguez, C. J.; Roth, G. A.; Rosamond, W. D.; Sampson, U. K. A.; Satou, G. M.; Shah, S. H.; Spartano, N. L.; Tirschwell, D. L.; Tsao, C. W.; Voeks, J. H.; Willey, J. Z.; Wilkins, J. T.; Wu, J. HY.; Alger, H. M.; Wong, S. S.; Muntner, P. Heart Disease and Stroke Statistics—2018 Update: A Report From the American Heart Association. *Circulation* **2018**, *137* (12). https://doi.org/10.1161/CIR.0000000000000558.

(2) Meischke, H.; Kuniyuki, A.; Yasui, Y.; Bowen, D. J.; Andersen, R.; Urban, N. INFORMATION WOMEN RECEIVE ABOUT HEART ATTACKS AND HOW IT AFFECTS THEIR KNOWLEDGE, BELIEFS, AND INTENTIONS TO ACT IN A CARDIAC EMERGENCY. *Health Care Women Int* **2002**, *23* (2), 149–162. https://doi.org/10.1080/073993302753429022.

(3) Martinez-Nadal, G.; Miro, O.; Matas, A.; Cepas, P.; Aldea, A.; Izquierdo, M.; Coll-Vinent, B.; Garcia, A.; Carbo, M.; Manuel, O.; Aguilo, S.; Esteban, E.; Lopez-Barbeito, B. An Analysis Based on Sex&Gender in the Chest Pain Unit of an Emergency Department during the Last 12 Years. *Eur Heart J Acute Cardiovasc Care* **2021**, *10* (Supplement_1). https://doi.org/10.1093/ehjacc/zuab020.122.

(4) Mayo Clinic Staff. *Myocardial ischemia*.

(5) Schmiedl, A.; Schnabel, Ph. A.; Richter, J.; Gebhard, M. M.; Bretschneider, H. J. The Contraction State of Myofibrils During Global Ischemia and After Reperfusion Following Different Forms of Cardiac Arrest. *Pathol Res Pract* **1994**, *190* (5), 482–492. https://doi.org/10.1016/S0344-0338(11)80211-6.

(6) Swank, D. M. Mechanical Analysis of Drosophila Indirect Flight and Jump Muscles. *Methods* **2012**, *56* (1), 69–77. https://doi.org/10.1016/j.ymeth.2011.10.015.

(7) Frontera, W. R.; Ochala, J. Skeletal Muscle: A Brief Review of Structure and Function. *Calcif Tissue Int* **2015**, *96* (3), 183–195. https://doi.org/10.1007/s00223-014-9915-y.

(8) Nucciotti, V.; Stringari, C.; Sacconi, L.; Vanzi, F.; Fusi, L.; Linari, M.; Piazzesi, G.; Lombardi, V.; Pavone, F. S. Probing Myosin Structural Conformation in Vivo by Second-Harmonic Generation Microscopy. *Proceedings of the National Academy of Sciences* **2010**, *107* (17), 7763–7768. https://doi.org/10.1073/pnas.0914782107.

(9) Kollmar, M. Crystal Structure of the Motor Domain of a Class-I Myosin. *EMBO J* **2002**, *21* (11), 2517–2525. https://doi.org/10.1093/emboj/21.11.2517.

(10) Tiaho, F.; Recher, G.; Rouède, D. Estimation of Helical Angles of Myosin and Collagen by Second Harmonic Generation Imaging Microscopy. *Opt Express* **2007**, *15* (19), 12286. https://doi.org/10.1364/OE.15.012286.

(11) Brawley, J.; Etter, E.; Heredia, D.; Intasiri, A.; Nennecker, K.; Smith, J.; Welcome, B. M.; Brizendine, R. K.; Gould, T. W.; Bell, T. W.; Cremo, C. Synthesis and Evaluation of 4-Hydroxycoumarin Imines as Inhibitors of Class II Myosins. *J Med Chem* **2020**, *63* (19), 11131–11148. https://doi.org/10.1021/acs.jmedchem.0c01062.

(12) Kobayashi, M.; Takatori, T.; Nakajima, M.; Saka, K.; Iwase, H.; Nagao, M.; Niijima, H.; Matsuda, Y. Does the Sequence of Onset of Rigor Mortis Depend on the Proportion of Muscle Fibre Types and on Intra-Muscular Glycogen Content? *Int J Legal Med* **1999**, *112* (3), 167–171. https://doi.org/10.1007/s004140050225.

(13) Boyd, R. W. *Nonlinear Optics*, 3rd ed.; Academic Press, 2008.

(14) Moreaux, L.; Sandre, O.; Blanchard-Desce, M.; Mertz, J. Membrane Imaging by Simultaneous Second-Harmonic Generation and Two-Photon Microscopy. *Opt Lett* **2000**, *25* (5), 320. https://doi.org/10.1364/OL.25.000320.

(15) Campagnola, P. J.; Millard, A. C.; Terasaki, M.; Hoppe, P. E.; Malone, C. J.; Mohler, W. A. Three-Dimensional High-Resolution Second-Harmonic Generation Imaging of Endogenous Structural Proteins in Biological Tissues. *Biophys J* **2002**, *82* (1), 493–508. https://doi.org/10.1016/S0006-3495(02)75414-3.

(16) Asadipour, B.; Beaurepaire, E.; Zhang, X.; Chessel, A.; Mahou, P.; Supatto, W.; Schanne-Klein, M.-C.; Stringari, C. Modeling and Predicting Second-Harmonic Generation from Protein Molecular Structure. *Phys Rev X* **2024**, *14* (1), 011038. https://doi.org/10.1103/PhysRevX.14.011038.

(17) Greenhalgh, C.; Stewart, B.; Cisek, R.; Prent, N.; Major, A.; Barzda, V. Dynamic Investigation of Drosophila Myocytes with Second Harmonic Generation Microscopy; Mathieu, P., Ed.; 2006; p 634308. https://doi.org/10.1117/12.706559.

(18) Plotnikov, S. V.; Millard, A. C.; Campagnola, P. J.; Mohler, W. A. Characterization of the Myosin-Based Source for Second-Harmonic Generation from Muscle Sarcomeres. *Biophys J* **2006**, *90* (2), 693–703. https://doi.org/10.1529/biophysj.105.071555.

(19) Prent, N.; Green, C.; Greenhalgh, C.; Cisek, R.; Major, A.; Stewart, B.; Barzda, V. Intermyofilament Dynamics of Myocytes Revealed by Second Harmonic Generation Microscopy. *J Biomed Opt* **2008**, *13* (04), 1. https://doi.org/10.1117/1.2950316.

(20) Samim, M.; Prent, N.; Dicenzo, D.; Stewart, B.; Barzda, V. Second Harmonic Generation Polarization Properties of Myofilaments. *J Biomed Opt* **2014**, *19* (5), 056005. https://doi.org/10.1117/1.JBO.19.5.056005.

(21) Harvey, M.; Cisek, R.; Alizadeh, M.; Barzda, V.; Kreplak, L.; Tokarz, D. High Numerical Aperture Imaging Allows Chirality Measurement in Individual Collagen Fibrils Using Polarization Second Harmonic Generation Microscopy. *Nanophotonics* **2023**, *12* (11), 2061–2071. https://doi.org/10.1515/nanoph-2023-0177.